Atomic aspects in the epitaxial growth of metallic superlattices and nanostructures

2002 J. Phys.: Condens. Matter 14 R1063

(http://iopscience.iop.org/0953-8984/14/43/201)

INSTITUTE OF PHYSICS PUBLISHING JOURNAL OF PHYSICS: CONDENSED MATTER

J. Phys.: Condens. Matter **14** (2002) R1063–R1097 PII: S0953-8984(02)35556-5

TOPICAL REVIEW

Atomic aspects in the epitaxial growth of metallic superlattices and nanostructures

J J de Miguel[1] **and R Miranda**

Departamento de Física de la Materia Condensada and Instituto de Ciencia de Materiales 'Nicolás Cabrera', Universidad Autónoma de Madrid, Cantoblanco, 28049 Madrid, Spain

E-mail: juanjose.demiguel@uam.es

Received 5 April 2002, in final form 29 August 2002
Published 18 October 2002
Online at stacks.iop.org/JPhysCM/14/R1063

Abstract

The properties of materials (mechanical, electronic, magnetic, etc) derive ultimately from the identity and spatial arrangement of their constituents. Nowadays, with the dimensions of technological devices and nanostructures reaching a few atomic constants, descriptions in terms of macroscopic concepts appear to be frequently inadequate and must give way to atomistic formulations based on elementary processes. Focusing on metallic materials, and more specifically on low-dimensional systems such as ultrathin films, superlattices or nanostructures, this paper reviews the atomic scale phenomena responsible for the most common types of defects (interfacial alloying, etching and roughness, formation of dislocations and pinholes, film discontinuities and twinning). It is shown that many of these features are related to the different mechanisms of strain relaxation in heteroepitaxial systems as well as to specific characteristics of atomic diffusion, such as the presence of Ehrlich–Schwoebel barriers hindering step crossings. Some special growth techniques (use of surfactants and codeposition) are also presented together with experimental examples demonstrating their usefulness to overcome the elements' natural limitations and produce accurately controlled, custom-designed epitaxial samples. Finally, a brief overview is given of different phenomena that can be exploited to produce self-assembled or self-organized structures.

Contents

[1] Author to whom any correspondence should be addressed.

0953-8984/02/431063+35$30.00

1. Introduction

The pioneering work by Esaki [1] opened vast prospects for electronic band engineering and, in general, greatly broadened the scope of modern materials science. The groundbreaking idea was to surmount the limitations imposed by being restricted to using only the equilibrium phases of materials and start designing metastable structures with custom-chosen properties. Since then, impressive advances have been made, especially in the field of semiconductor materials [2]. This is basically due to the predominantly covalent nature of their bonding (directionality, localization, possibility to tailor misfit accommodation through manipulation of the chemical composition in III–V or II–VI compounds, etc) that facilitates the growth of well-defined, low-dimensional structures. The situation is far more complex when we turn to metals. The basic characteristics of the metallic bond (delocalization, isotropy, etc) create formidable difficulties in controlling the arrangement of atoms in artificial materials, hampering the realization in practice of many theoretical predictions.

The uninterrupted efforts devoted over the last decades to continuously reduce the dimensions of devices have led us to the current burst of activity centred on nanoscale science and technology. Nowadays the subjects of both basic research and state-of-the-art development are frequently systems with atomic scale dimensions. We have therefore reached a point where macroscopic criteria are no longer valid, and a detailed knowledge of the atomistic processes taking place during the preparation of these materials is a must.

Soon after the first thermodynamic treatment of surface structure and growth, due to Gibbs [3], atomistic formulations of the problem appeared [4, 5]. The BCF theory of crystal growth [6] was the culmination of this process, laying the foundations of our present-day knowledge. This kind of model has been boosted in recent times by advances in both computational and experimental techniques. The former now allow us to treat ensembles of moderately large numbers of atoms, thus furnishing increasingly realistic approximations to real systems. As for the latter, some have reached true atomic resolution, as in the case of scanning tunnelling microscopy (STM) and can provide direct views of surface morphology with an unprecedented level of detail. The progress achieved by other techniques, such as x-ray diffraction (XRD) using modern synchrotron sources, is also remarkable, being now capable not only of solving static structures, but also of monitoring dynamical processes in real time. All in all, researchers today have available an increasing wealth of information relating macroscopic materials properties to their basic structure and morphology, which in turn stem from very fundamental processes at the atomic scale.

The purpose of this review is to help sort out this information by reviewing recent experimental and theoretical results revealing the atomistic phenomena that appear to be most influential on the final constitution of epitaxial heterostructures. Restricting ourselves

to metallic systems, in the following sections we will survey the different mechanisms of interfacial alloying and also several effects directly related to specific features of atomic diffusion, such as kinetic roughening and step bunching. We will also discuss some special methods which are particularly efficient to face these difficulties and improve the epitaxial growth of those systems. This review will be concluded with a short section devoted to presenting recent significant results on the creation of spontaneously ordered (self-assembled or self-organized) low-dimensional structures. This account is not meant to be an exhaustive catalogue of previously available data; the intention is rather to illustrate the fundamental physical principles, common to a wide variety of systems.

2. Interdiffusion

For a long time, the substrate surface was considered an inert template whose role during epitaxial growth was, at most, to dictate the structure and symmetry of the epilayer [7]. Based on this assumption, many efforts were launched to produce artificial materials and realize the theoretical predictions about their exotic properties. However, reality proved to be more complex, and many of those attempts did not come up to expectations. More careful work on the structural characterization of the samples and the progress achieved in recent years in analytical techniques revealed a wealth of unexpected features. Most notably, the arrival of STM [8] revolutionized the field and offered us direct views of the atomic structure of epitaxial films.

Regarding interface formation and mixing, it has become clear that bulk phase diagrams are not a valid guide. On the contrary, it is now generally accepted that interdiffusion is much more ubiquitous than it was previously thought. And, most importantly, chemical interactions between the different species of atoms are not the only cause of atomic intermixing: for instance, strain, a hardly avoidable element in heteroepitaxial systems, also plays an important role. Moreover, the mixing process does not involve necessarily only individual atoms: several reports have shown interdiffusion associated with the dynamics of adsorbate islands. We shall now discuss these phenomena in some detail.

2.1. Single atoms

2.1.1. Mixing at terraces. In an atomistic view of the deposition and alloying process, this can be considered the basic mechanism. Obviously, the formation of an alloyed interface should be expected whenever the two materials put in contact are miscible in bulk. Nevertheless, even this criterion must be handled with care. It has been shown that the charge transfer between an epitaxial overlayer and the substrate can be completely different, and even of opposite sign, with respect to the bulk materials [9]. This is a consequence of the electronic band narrowing caused by the reduced dimensionality and coordination of the deposit. Besides, on calculating the Gibbs' free energy of the mixed system to decide whether the alloying process is favoured, configurational entropy can be very different in surfaces or interfaces and in the bulk [10, 11].

Open crystal faces such as the fcc-(100) are prone to show diffusion by the atomic exchange mechanism [12, 13] (this subject will be dealt with in detail in section 3.1). Thus, any species deposited on these type of surfaces is likely to form a substitutional alloy confined to the interface. Many examples can be found in the literature, among which one could mention Mn/Cu(100) [14], Pd/Cu(100) [15], Mn/Ag(100) [16] or Co/Cu(100) [17, 18]. In many cases interdiffusion proceeds from the substrate steps, because the increased mobility of edge and kink atoms allows for an easier penetration of the deposit.

Strain effects due to lattice mismatch must also be taken into account: the elastic energies present in misfitting systems can be comparable to those associated with atomic diffusion

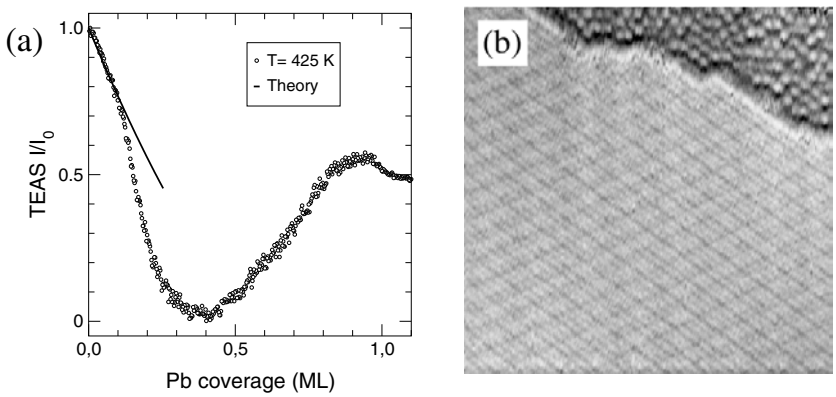

Figure 1. (a) Evolution of the specular TEAS intensity during deposition of 1 ML of Pb on Cu(111) at 425 K. From the exponential fit to the low coverage region below the break at 0.14 ML, a cross section for diffuse scattering Σ_{Pb} of $\sim$26 Å^2 per Pb atom is found. Such a small value reveals that the Pb atoms are inserted within the Cu surface rather than adsorbed on it. (b) STM micrograph (160×160 Å^2) showing the coexistence of regions containing dispersed Pb atoms alloyed within the Cu surface (upper right corner) and others with the $p(4 \times 4)$ superstructure of the compact Pb monolayer formed after dealloying. The Pb coverage is 0.65 ML (image courtesy of R Otero and A L Vázquez de Parga.)

and adsorption [19]. An empirical criterion including different energetic contributions has been proposed to decide whether two materials will mix at their interface [20–22]. Recent total energy calculations [11] have confirmed most of the predictions issued by this model. A treatment due to Tersoff [23] gives us some physical insight into the driving forces for alloying of immiscible metals. Surface atoms have a reduced coordination, and therefore they benefit from the insertion of larger ones, which allows them to gain the electronic density they need [10]. The inserted atom also lowers its energy by increasing its bonding. The strain due to lattice mismatch can be easily relieved at the surface; this model thus predicts the formation of a dispersed surface alloy in most systems with relatively large differences in atomic size and for low adsorbate coverages [23]. With increasing thickness, the different atomic sizes and the difficulties of accommodating strain forbid bulk miscibility [24] and therefore spontaneous de-alloying is expected. The experimentally observed mixing of Au/Ni(110) [25], Ag/Pt(111) [26], Rh/Au(111) [27], Ni/Ag(111) [28] or Ag/Cu(100) [29], to mention just a few representative cases, can be understood along these lines.

The main features of this model are nicely demonstrated by experiments such as the growth of Pb on Cu(111). Due to the large lattice mismatch between these two materials (37%) Pb grows on Cu(111) at room temperature (RT) in the Stranski–Krastanov mode [30], forming a single wetting monolayer followed by three-dimensional islands. Figure 1(a) shows a Pb uptake curve measured by means of TEAS (thermal energy atom scattering). Here we monitor the variations of the specularly diffracted intensity of a beam of neutral He atoms in real time during Pb deposition; the substrate temperature was 425 K in this case, and the intensity has been normalized to the reflectivity of the bare Cu(111) surface. The large sensitivity of TEAS for surface defects allows us to follow in great detail the evolution of surface morphology.

The initial intensity drop (below a coverage $\Theta_{Pb} \simeq 0.39$ ML) indicates that disorder is steadily increasing on the surface. Then the reflectivity recovers as Pb deposition continues and the empty sites within the growing layer progressively get filled. At this stage a compact Pb layer is forming, with hexagonal symmetry and a saturation coverage of 71% of the Cu(111)

face; this corresponds roughly to the lattice constant of bulk Pb. The maximum diffracted intensity is reached once this incommensurate layer is completed. After that, additional atoms penetrate into the Pb layer, whose nearest-neighbour distance decreases until it becomes commensurate with the Cu(111) substrate [31, 32]. The compressive strain accumulated by the Pb layer is relieved at least partially by vertical displacements of the atoms in the Pb and the uppermost Cu layers. A buckled unit cell thus results, with a $p(4 \times 4)$ superstructure and containing 3 Pb atoms for a saturation coverage of $9/16$, which we choose as the definition of the Pb monolayer. Beyond this point large 3D islands of bulk-relaxed Pb start to appear, with separations of the order of hundreds of nanometres [33].

A more detailed inspection of the data in figure 1(a) reveals a break in the slope of the reflectivity curve at a Pb coverage of 0.14 ML. This is unambiguous evidence for a change in the cross section for diffuse scattering Σ_{Pb} of the Pb atoms adsorbed on the surface. This cross section measures the area whose electronic density is distorted by the presence of the adsorbate in such a way that the incoming He atoms are no longer scattered into the specular direction. Experimentally, the value of Σ_{Pb} can be determined by assuming random adsorption and fitting the initial drop of intensity with the expression [34]

$$I/I_0 = \left[1 - \frac{n_{\mathrm{A}}}{(n_{\mathrm{S}}/m)}\Theta\right]^{(n_{\mathrm{s}}/m)\ \Sigma_{\mathrm{A}}}. \tag{1}$$

In this equation, Θ is the adsorbate coverage, n_{A} (n_{S}) is the atomic density of the adsorbate (substrate) and m takes into account the number of sites allowed for adsorption due to geometrical reasons; in this case, the large size of Pb atoms precludes the occupation of all neighbouring positions and hence $m = 3$. Typical values for the cross section of isolated metal adatoms range around 100 Å^2 [35]. Nevertheless, the fit to our data (full curve in figure 1(a)) yields a much smaller value, $\Sigma_{\mathrm{Pb}} = (25.8 \pm 0.5)$ Å^2. A previous study of Pb on Cu(100) [36, 37] also found a cross section of $\sim$24 Å^2 for Pb atoms adsorbed at the substrate steps and partly shadowed by them. However, the step density in the Cu(111) substrate cannot account for the high coverage reached by this structure. The explanation for this effect finally came from STM experiments [38] which demonstrated the existence of a dispersed surface alloy, with Pb atoms inlaid within the Cu surface and separated from each other by a few lattice sites. This behaviour not only follows closely the predictions of Tersoff's model for the dilute alloy phase [23]; with further deposition one can also observe the expected de-alloying of the embedded Pb atoms. The STM image presented in figure 1(b) corresponds to a Pb coverage of 0.65 ML, and it shows a region on the surface (upper right corner) where the alloy coexists with the compact hexagonal layer that is growing at its expense. This phase is very homogeneous and sits directly on the Cu substrate; as its islands spread across the surface the buried Pb atoms are pulled out of the alloy layer and incorporated into them. Structural determination studies performed by means of dynamical LEED calculations [39] have shown that this de-alloying process is complete: when the commensurate, $p(4 \times 4)$ structure covers the whole surface all Pb atoms are confined to the overlayer, although the buckling induced by the latter affects several Cu planes.

One can thus conclude that this type of dilute, surface-confined alloying between large-mismatch elements might be common. This factor can seriously degrade the first stages of heteroepitaxial growth and hamper the preparation of nanostructures. On the other hand, it does not seem to be too much of a problem for the growth of thin films or superlattices, thanks to the spontaneous de-alloying taking place before completion of the first monolayer.

2.1.2. Step insertion. Step sites are particularly reactive positions, as demonstrated by their intense catalytic activity [40], the reason being the large number of unsaturated bonds of the

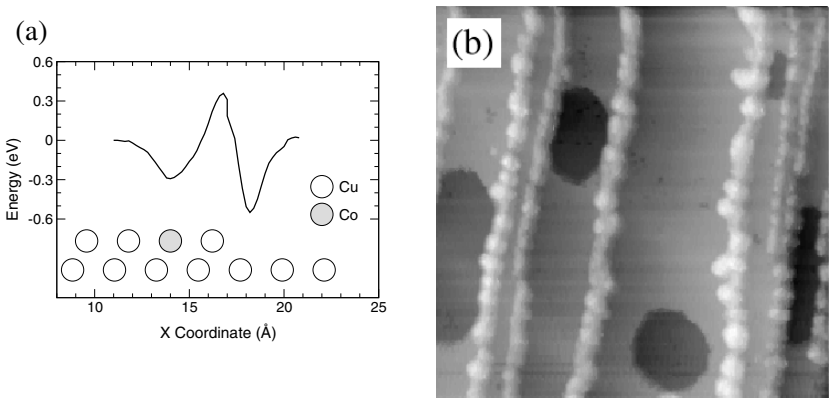

Figure 2. (a) Adsorption energy for a Co adatom moving perpendicularly to an atomic step on Cu(111), with another Co atom (shaded circle) inserted in the Cu terrace near the edge. The energy curve has been obtained by static relaxation using EAM interatomic potentials and shows an attractive well above the intermixed Co atom [45]. (b) STM image, 500 × 500 Å^2 in size, showing wires of Co–Cu grown on vicinal Cu(111) by exploiting the preferential nucleation at those positions, near descending steps [49].

edge atoms. Their reduced coordination is also responsible for the large relaxations that the positions of these atoms can suffer. This feature manifests itself in several different ways: for instance, it seems that diffusing adatoms always cross steps by a process similar to the atomic exchange observed in some surfaces [12]. Upon reaching a descending step, the diffusing adatom pushes out and replaces an edge atom, even on close-packed surfaces on which in-plane diffusion takes place by hopping [41, 42]. Obviously, this process can be considered as much a special case of intermixing as a mechanism of interlayer diffusion. Calculations for the deposition of Co on Cu(111) using embedded atom (EAM) interatomic potentials show that the energy of a single Co atom inserted within the Cu surface layer close to a step can be up to 0.19 eV lower than when simply stuck to the ascending edge [43]. This gain in energy is made possible by the specially efficient ability of the atomic rows in the vicinity of the step to relieve the strain caused by the insertion of other lattice-mismatched species. In contrast, the burrowing of a Co atom in the middle of the Cu(111) terrace, far away from the step, is usually not observed.

Several reports on preferential mixing at steps exist in the literature, both theoretical and experimental. Monte Carlo (MC) and molecular dynamics (MD) simulations for Ni/Cu(111) [44] and Co/Cu(111) [45] favour adatom insertion into the edge from the upper terrace as the preferred mechanism; incorporation from the lower side seems to be less efficient. The latter study also found, by static relaxation with EAM potentials, that Co atoms buried near the edges act as preferential binding sites for other Co atoms, with an adsorption energy of about 0.30 eV. The result of this calculation is depicted in figure 2(a). Similar results (0.34 eV) were obtained with density functional theory (DFT) calculations [18] for isolated Co atoms buried in a Cu(100) surface. Nucleation of islands near descending steps has also been observed in experiments on Cr/Pt(111) [46] or Fe/Cu(111) [47] and even in other, apparently unrelated systems such as LiF/Ag(111) [48]. This effect has been used to grow arrays of magnetic quantum wires of Co on vicinal Cu(111) surfaces [49], such as the ones shown in figure 2 (b). This STM image has a size of 500 × 500 Å^2; the clusters that decorate the substrate steps have double atomic height measured from the upper terrace and they contain a mixture of the deposited Co and Cu etched from the surface. The formation of these clusters is a collective phenomenon involving break-up of Co islands; it will be discussed in detail in the next section.

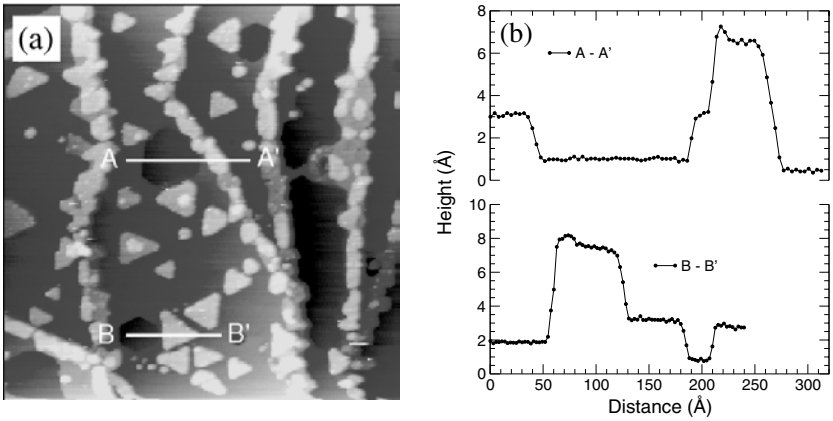

Figure 3. (a) STM image of a submonolayer deposit of Co grown at room temperature on Cu(111) (courtesy of J E Prieto and J de la Figuera). These two materials are immiscible in volume; nevertheless, the decoration of all surface steps with irregularly shaped clusters and the presence of islands of vacancies are hints of interdiffusion and surface etching. (b) Height profile taken along the straight lines marked in the STM image, showing that the islands have double atomic height, a feature also caused by interfacial alloying.

2.2. Collective mechanisms

In the examples described so far the deposited atoms mix with the substrate individually. Nevertheless, there exist also reports of intermixing occurring only after the formation of adsorbate islands or in their vicinity. In some cases, intermixing takes place at island edges, where the substrate atoms are pulled out of the surface as the island tries to relax [50].

Other instances of interdiffusion associated with aggregates of atoms have a profound influence on surface morphology and deserve an in-depth overview. The growth of Co on Cu can again be taken as a prototypical example. As we have seen in the previous sections, in the more open Cu(100) face atomic exchange processes are relatively easy, and Co adatoms can readily mix and occupy substitutional sites in spite of these two materials being bulk-immiscible. On the contrary, the Cu(111) face is much more compact and flat; both MC and MD simulations have shown that Ni [44] and Co [45] atoms diffuse by hopping and never mix except at the substrate steps. Nevertheless, STM pictures like the one displayed in figure 3(a) reveal a completely different situation. This image has 1000 Å on each side, and shows the typical status of the Cu(111) surface after deposition of 0.3 ML of Co at room temperature. A number of features visible on the surface are indicative of extensive interdiffusion. The graphs in figure 3(b) show the topographic profiles along the lines AA′ and BB′ marked on the STM image. It is clear from these transverse cuts that the irregular clusters decorating the surface steps and the triangular islands nucleated across the terraces have double atomic height. They contain a mixture of Co and Cu, as determined by ISS [51] and CO titration experiments [52]. On the surface there also exist islands of vacancies of single atomic depth, resulting from surface etching.

The microscopic mechanisms responsible for the appearance of these structures have been unravelled by means of computer simulations [45]. These latter techniques are becoming an increasingly helpful tool to analyse complex atomistic problems, thanks to advances in computational power and the availability of potentials allowing for realistic descriptions of atomic interactions [53]. The many-body, second-moment approximation of the tight-binding scheme (TB-SMA) potentials [54] used in this case have proven capable of reproducing a

variety of experimental observations [55, 56]. From MC simulations in continuous space with this set of interactions a surprising picture emerges. Confirming the previous results mentioned above, Co adatoms diffuse by hopping on flat Cu(111) terraces and nucleate islands of single atomic height. These islands grow in size as additional Co atoms arrive from the 2D gas phase and stick to their borders. Upon reaching a critical size (about 25 atoms) the Co islands become unstable and break up. The process is schematically portrayed in figure 4, where the evolution of both the Co island (shaded circles) and the Cu substrate (open circles) is shown in both top (left column) and side view (right). These snapshots demonstrate how the island starts to swell upwards at its centre, while at the same time pulling from the Cu atoms below it. A few of these substrate Cu atoms are actually drawn out of the surface layer and mix with the Co. In the final state, the island contains Co and Cu atoms distributed in two atomic layers with some vacancies left in the substrate. This picture closely mirrors the main features observed in the STM image of figure 3(a). As for the driving force behind the island break-up, recent total energy calculations point toward the strain accumulated by the Co atoms forced to grow pseudomorphically on a relatively soft Cu(111) substrate [57]. One can therefore expect this kind of behaviour to be very common among heteroepitaxial systems. In fact, double-atomic-height islands at the interface have been reported for many systems, such as Co/Cu(111) [52], Co/Cu(100) [58, 59], Fe/Cu(111) [60] or Co/Au(111) [61].

While real-space images like those furnished by STM are easier to interpret, diffraction measurements offer other advantages. In most cases, they can be taken in real time during growth, they probe a relatively large sample area and provide a statistical average of the surface morphology. From the analysis of those data, a great deal of information on the growth process can be inferred [62]. Among the different diffraction techniques commonly employed, TEAS is particularly useful. It combines high surface sensitivity, non-damaging atom–surface interaction and purely kinematic scattering.

Figure 5 demonstrates the kind of information that can be obtained from such experiments. Uptake curves were measured at different incidence angles during the deposition of Co on Cu(100) at RT [63]. For a comprehensive analysis of the data, all these curves were put together in order to construct the 3D plot shown in figure 5(a) [64, 65]. Looking at the evolution of the TEAS intensity as a function of film thickness for a fixed incidence angle (full white line), one can easily observe the characteristic periodic oscillations revealing layer-by-layer (LBL) growth of the deposit in figure 5(b) [66–68]. As expected, these oscillations are more clearly visible when the incidence angle of the primary He beam corresponds to out-of-phase conditions for terraces separated by monoatomic steps. One must notice, however, that the first oscillation is anomalous for all incidence angles. Taking cuts on the intensity surface at constant coverage (broken white lines in figure 5(a)) effective $\theta - 2\theta$ scans can be obtained for any desired film thickness. These curves are plotted in figure 5(c) as a function of incidence angle; applying Bragg's law [69] one finds from them that the angular positions for in-phase and out-of-phase interference change during growth. At half-monolayer coverage (top curve), they reveal a step height of 4.1 Å, corresponding to the double-atomic-height islands mentioned above. With further deposition the Cu surface gradually gets covered and interdiffusion comes to an end; single-layer Co islands are stable when formed on a Co substrate. The $\theta - 2\theta$ scan for 1.5 ML of Co (middle curve) shows how the interference conditions are shifting towards their final positions, which are reached already for 2.5 ML thickness (bottom curve) and correspond to an interlayer spacing of 1.74 ± 0.04 Å. This is slightly smaller than the bulk Co value (1.77 Å), a contraction in the direction perpendicular to the surface that can be explained by the in-plane expansion resulting from growing pseudomorphically with the Cu substrate. Thus, this type of experiment can provide a full description of the surface morphology and its evolution at all times during growth.

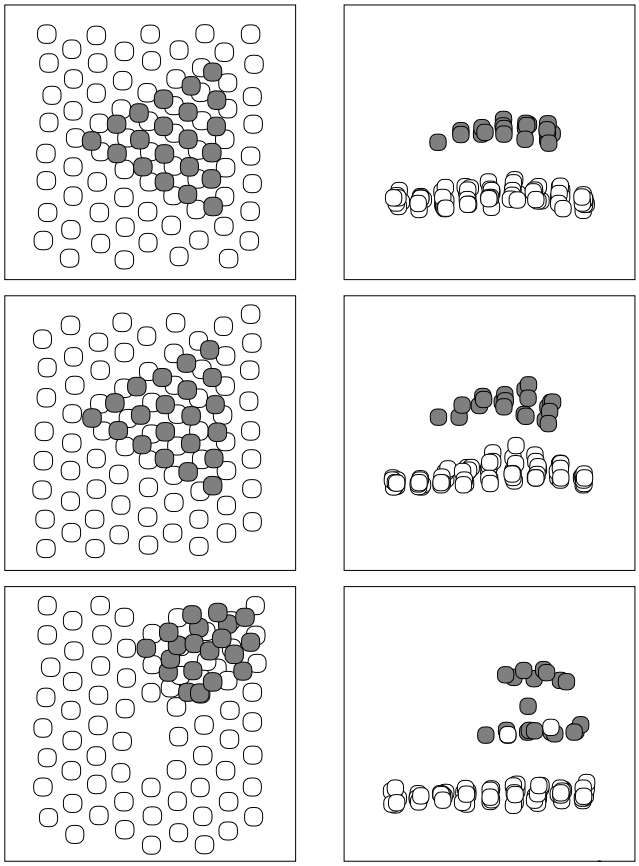

Figure 4. MC simulation of the break up of a heteroepitaxial Co island (●) of single atomic height on Cu(111) (○). The side view in the right-hand panels shows that the island instability develops mainly at its centre, pulling some Cu atoms out of the surface layer. The vacancies left by this process can be seen in the top view presented in the left-hand panels (taken from [45]).

The clusters decorating the atomic steps in figure 2(b) also have double atomic height measured from the upper terrace, and they have been formed in the same way: the islands nucleated initially above the buried Co atoms near the steps reach the critical size, explode and form the Co–Cu aggregates decorating the edges and pools of vacancies confined between consecutive steps. The irregular shape of the clusters probably results from the coalescence of adjacent islands at early stages after their appearance and before diffusion along their borders can smooth them out. The limited incorporation of adatoms, due to the island's position near the terrace edges, also favours the permanence of rough edges and malformed shapes, similar to the ones observed in the last snapshot of the simulation shown in figure 4. Islands of double atomic height nucleated at the upper edge of atomic steps have also been observed for Cr/Pt(111) [46].

The collective mechanisms of interdiffusion discussed in this section pose additional severe limitations for the preparation of well-defined interfaces. They are related to the accommodation of misfit, an ingredient that is inherent to almost any heteroepitaxial system. There is a clear need to develop novel growth techniques that may allow us to overcome these difficulties. Several possible candidates will be reviewed in section 4.

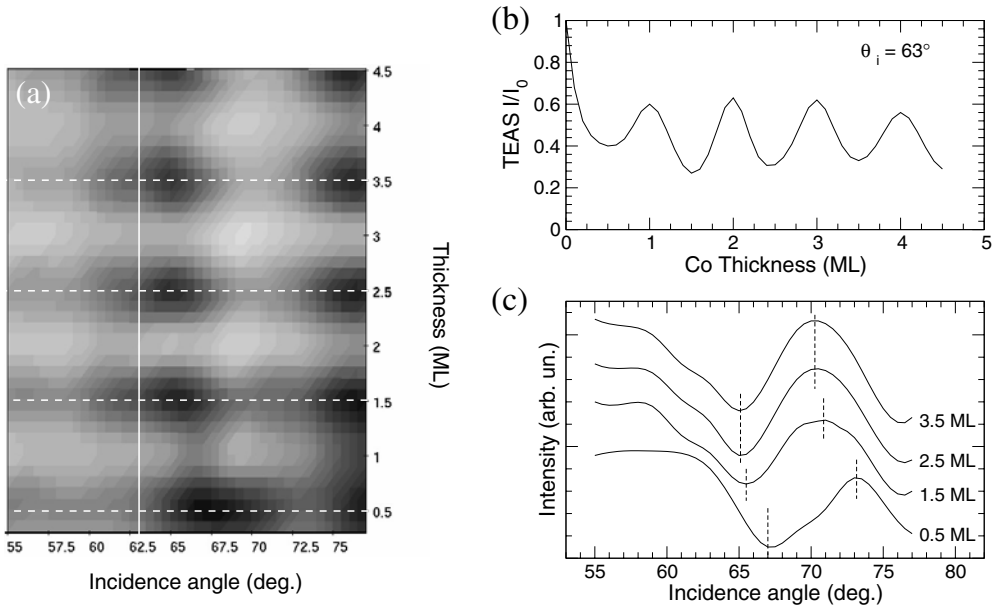

Figure 5. (a) Representation of the specularly diffracted TEAS intensity as a function of both incidence angle and deposited thickness during growth of Co on Cu(100) at RT. (b) Taking a cut in the 3D intensity plot at constant incidence angle, an uptake curve is obtained that displays the characteristic oscillations representative of LBL growth. (c) Transverse cuts, taken at constant coverage, show shifts in the angular positions corresponding to in-phase and out-of-phase scattering, indicative of the elastic relaxations suffered by the Co film to accommodate the misfit strain [65]

3. Atomic diffusion

This is another example of a fundamental phenomenon of which our understanding has been essentially altered in recent years. Modern theoretical [70] and experimental techniques [71] have found evidence for complex phenomena such as long-distance jumps [72–74] or islands and cluster diffusion [75–77]. Substrate-mediated long-range interactions between adatoms have also been shown to influence their motion [78, 79].

Research on the field of surface diffusion has been maintained in a very active state for a long time, and a vast amount of literature is available [80]. Readers seeking more exhaustive information are referred to some of the excellent reviews available [81]. In this work we shall focus on the aspects that we consider most influential with respect to the final morphology of metallic superlattices and nanostructures.

3.1. In-plane diffusion

Traditionally, diffusing adatoms were pictured moving on a more or less rigid surface, hopping from a low-energy adsorption site to another through bridge positions. This view was first questioned on the basis of experimental observations [13] that soon received a theoretical interpretation [12]. These studies unveiled the existence of an alternative mechanism, termed *atomic exchange*. In this mode the moving atom replaces another one inside the surface layer rather than jumping over the substrate. In homoepitaxy, the result after a few of these events is a net displacement of an atom with respect to the original landing site; but in the case of heteroepitaxial systems exchange diffusion causes a frequently undesirable amount of interfacial mixing.

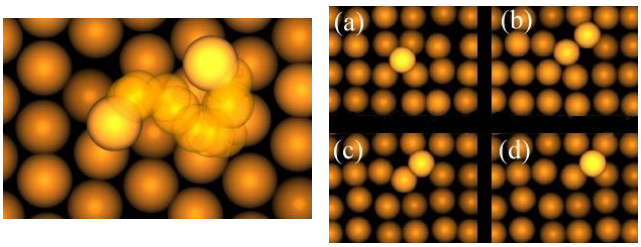

Figure 6. Mechanisms of atomic diffusion: hopping over the Cu(111) surface (left) and site exchange on Cu(100) (right). The images are snapshots of MC simulations run using tight-binding, second-moment (TB-SMA) many-body interatomic potentials [55, 56, 82].

Table 1. Summary of activation energies reported for surface self-diffusion on Cu(100). All values are in eV.

Hopping	Exchange	Experiment	Reference
0.48	0.80	—	[88]
0.45	—	—	[89]
0.53	0.79	—	[90]
0.49	>1	—	[91]
0.38	0.72	—	[90]
0.66	—	—	[92]
0.47	0.43	—	[93]
0.42	0.23	—	[94]
0.49	0.69	—	[95]
—	—	0.48 ± 0.08	[69]
—	—	0.39 ± 0.06	[96]
—	—	0.28 ± 0.06	[97]
—	—	0.36 ± 0.03	[98]

These two basic mechanisms are illustrated in figure 6. The image on the left-hand side shows the trajectory of a Cu atom self-diffusing over a Cu(111) surface. It has been obtained by means of a MC simulation with the same TB-SMA interatomic potentials described in the previous section [55, 56, 82]. The right-hand side of the same figure, in turn, presents an exchange event on Cu(100): the different frames depict characteristic surface configurations during the substitution process.

The appearance of exchange diffusion can be understood qualitatively by making use of very simple energetic arguments: during atomic exchange the coordination of the diffusing adatom is higher than at the bridge position that must be crossed for hopping. Therefore, the saddle point energy can be considerably lower for the former process, at least on open surfaces for which the activation energy for hopping diffusion is relatively high. Nevertheless, the displacement of the involved atoms must take place in a concerted way; the final balance of energy depends critically on very fine details of this movement. Theoretical predictions are complicated for this reason, and *ab initio* calculations have only recently started to be available [83]. Identifying exchange diffusion experimentally is also complicated; so far, it has only been possible by means of nuclear spectroscopy (perturbed angular correlation—PAC) [84] and FIM measurements [13, 85], these latter limited to refractory metals.

To illustrate the subtleties and complexity of this problem we will now briefly review the case of Cu(100). This face is a potential candidate for exchange diffusion, since all direct observations of this phenomenon reported to date occurred on fcc-(110) or (100) faces like it:

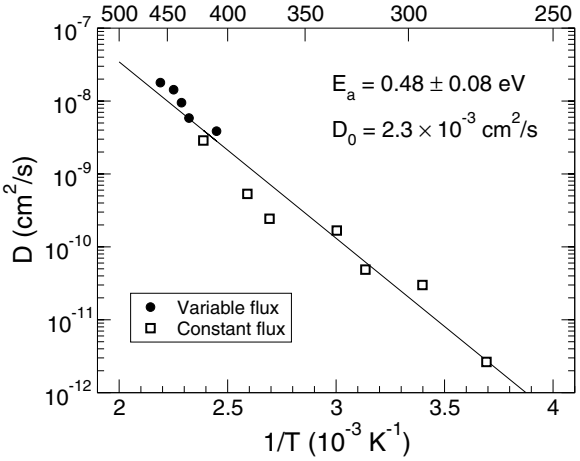

Figure 7. Surface diffusion coefficient for Cu(100) as derived from TEAS experiments of homoepitaxial growth using the two different methods described in the text [69]. An activation energy $E_a = 0.48 \pm 0.08$ eV is found from the slope of the Arrhenius fit.

Pt, Ir/Pt(110) [86], W/Ir(110) [87], Pt/Pt(100) [13] or Ir/Ir(100) [85]. Theoretical calculations on this system have been abundant but inconclusive; the results of a number of them are listed in table 1. Clearly, there is a much better agreement regarding the value of the activation energy for hopping diffusion than about exchange. This is so because the former is a much simpler process to describe: the trajectory is quite evident and involves only three atoms in practice. On the contrary, during exchange two atoms perform a concerted, simultaneous displacement of similar magnitude, with all their neighbours participating in some degree, as the series of snapshots in the right-hand panel of figure 6 demonstrates. Furthermore, the activation energy for exchange seems to be extremely sensitive to small contributions to the system's total energy, such as the one-electron correction, that are frequently neglected in the calculations [94].

From the experimental point of view, direct observations by means of FIM are unfeasible on a soft metal like Cu. Therefore, the information about surface diffusion on this substrate has been obtained by indirect means, analysing growth data with appropriate models. A first TEAS study examined the homoepitaxy on Cu(100) in a temperature range between 270 and 460 K [69]. This work combined two different approaches to determine the surface diffusion coefficient, which is depicted in figure 7 in an Arrhenius plot. The data points labelled with filled circles were obtained using different deposition rates and varying the substrate temperature until the step-flow growth mode was attained. The adatom mean free path λ is related to the diffusion coefficient D through the Einstein relation:

$$\lambda = \sqrt{D\tau} \tag{2}$$

where τ is the time spent by the atom moving freely on the surface. Considering that step flow growth takes place when the adatoms' diffusive length equals the average terrace size Λ, then τ corresponds to the average time interval between the arrivals of two consecutive atoms from the gas phase at the same terrace. Its value is thus directly related to the deposition rate F and the diffusion coefficient can be readily obtained [69, 99]:

$$\Lambda = \lambda = \sqrt{\frac{D}{F\Lambda^2}} \Rightarrow D = F\Lambda^4. \tag{3}$$

The average terrace size (or, equivalently, the step concentration on the surface) can easily be deduced from the scattered intensity by applying kinematic diffraction theory [62, 69, 100].

The second set of data (depicted with open squares) were obtained using a fixed deposition rate and different substrate temperatures. Again in this case it is assumed that the adatom mean free path equals the average distance between steps at the steady state reached once the initial intensity oscillations have decayed. Both sets of data show a remarkable agreement, and from their Arrhenius fit an activation energy for surface diffusion, $E_a = (0.48 \pm 0.08)$ eV, is found. This value agrees well with most of the theoretical results for the hopping mechanism (see table 1).

Another TEAS experiment, performed within a lower temperature range (140–250 K), arrived at a different conclusion [97]. By analysing the wings in the specularly diffracted intensity and relating their position in reciprocal space to the average distance between Cu islands nucleated on the same Cu(100) surface, Ernst *et al* found $E_a = (0.28 \pm 0.06)$ eV. One may be tempted to interpret the remarkable agreement between this result and the prediction of Hansen and coworkers [94] for exchange diffusion (see table 1) as a signal for a change in the diffusion mechanism, with exchange operating at low temperature and hopping dominating above ∼270 K. The controversy seemed to be settled when a more detailed reanalysis of these data found an activation energy of 0.40 eV, in much better agreement with the other experimental results and also with most of the theoretical ones. Furthermore, an *ab initio* study pointed out that exchange diffusion is to be expected only on the fcc-(100) faces of heavy elements, but not on the light ones such as Cu [83]. Nevertheless, taking into account the effect of temperature revived the discussion. In fact, a crossover from one diffusion regime to the other as a function of temperature is in general to be expected: the different activation energies imply that, in the Arrhenius representation, there will be two straight lines with different slopes that must intercept at some point; for Cu on Cu(100) the transition is expected to lie at about 750 K [101]. In the absence of conclusive experiments, this question remains open. However, this is an important piece of knowledge: for the purpose of growing chemically abrupt interfaces it is desirable to avoid the exchange regime by choosing the appropriate temperature range, if possible. An alternative solution might be to find ways to favour hopping over exchange. Recently, Kellogg [102] found that adsorbing hydrogen on Pt(100) could suppress exchange self-diffusion and force hopping. This can be considered a case of the surfactant effect, a subject that will be discussed in depth in section 4.1.

3.2. Barriers for interlayer diffusion

The so-called Ehrlich–Schwoebel (ES) barrier is defined as the supplementary energy that a freely diffusing adatom must overcome in order to cross a descending atomic step [103, 104]. This is a simplified description of a complex phenomenon. For instance, while terrace diffusion might occur either by hopping or exchange as mentioned above, step crossings seem to always take place by the push-out and roll-down mechanism described in section 2.1.2. Also, the relaxations of atomic positions close to the edges provoke alterations in the distribution of electronic density that in turn affect the potential energy landscape on which the atoms move. All these factors contribute to making diffusion near and across steps different from that occurring on flat areas far from them. The actual situation is schematically depicted in figure 8, as revealed by carefully monitoring the displacements of free adatoms near descending steps with FIM [105].

The presence of high ES barriers obviously causes reduced interlayer diffusion and rough growth fronts. With step crossings forbidden, growth typically results in surface morphologies such as those illustrated by figures 9(a) and (b). The first STM image covers 1000×1000 Å^2 in size and corresponds to 5 ML of Cu deposited on Cu(111); the second one is for 5 ML of Co on the same surface, and it measures 500×500 Å^2. Both films were grown at RT. The area exposed

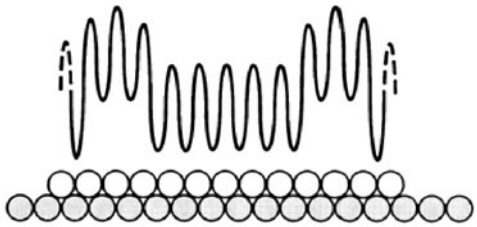

Figure 8. Schematic representation of the diffusion barriers across an atomic island. The higher energy required to cross the edges is often described in a simplified way in terms of an effective ES barrier (from [105]).

within each atomic layer in the latter image is plotted with vertical bars in figure 9(c); it clearly follows the Poisson distribution (full line) expected for random deposition and negligible interlayer diffusion [52]. One must notice the extremely high roughness accumulated for such a low deposited thickness, even for homoepitaxial growth. The deep gorges visible in the images appear as a result of island coalescence; they are very difficult to fill, since only atoms landing directly on them can do it. This effect has been shown to be most significant for compact crystalline faces such as the fcc-(111) or the bcc-(110) [106]; some examples are Cu/Cu(111) [107], Co/Cu(111) [52], Fe/Fe(110) and W/W(110) [108]. On these surfaces in-plane diffusion is very fast and hence the presence of the ES barrier establishes a larger asymmetry between the activation energies for terrace and interlayer diffusion [109, 110]. To put it in a more graphical way, free adatoms spend a very short time close to the step trying to cross the edge; soon, after a few unsuccessful attempts they move away from it and eventually meet other adatoms to nucleate an island on their original atomic level. In contrast, LBL growth is usually observed on more open faces such as the (100) [63, 69], because their rates of diffusion within the terraces and across the edges are not so different. The seemingly counter-intuitive conclusion is thus that slow surface diffusion allows for better two-dimensional growth.

Film morphologies, such as those observed in figures 9(a) and (b), are clearly unacceptable for the preparation of superlattices or any other kind of nanostructure that requires a fine control of shape and thickness. It is therefore necessary to develop growth methods that cope with these difficulties and induce LBL growth in systems with high ES barriers. The use of surfactants is perhaps the most successful one so far; it will be discussed in section 4.1. The heteroepitaxial case is further complicated by the coexistence of different crystallographic phases: Co, for instance, tends to adopt its equilibrium hcp structure by making stacking faults on the fcc-Cu(111) substrate [111, 112]. The lateral shift introduced between faulted and unfaulted islands provokes additional discontinuities in the films. Besides, the transition takes place gradually, with crystallites of the new phase appearing randomly at different positions across the sample and for a range of thicknesses spanning several monolayers [113]. In this way, structural coherence is lost within the film, also degrading the quality of subsequent layers during the growth of superlattices. Recent studies [114, 115] have demonstrated how to stabilize particular crystallographic phases (e.g. fcc-Co, fcc-Fe, etc) by codepositing the element of interest together with another one (e.g. Cu) that dictates the chosen structure. This procedure is described in more depth in section 4.2.

The absence of efficient interlayer diffusion does not manifest itself only during growth, but it also affects in a substantial way the morphology of clean surfaces. Already the earliest theoretical studies on the effect of ES barriers focused on their influence on step propagation, showing that kinetic step bunching can appear [116]. The mechanism is shown schematically

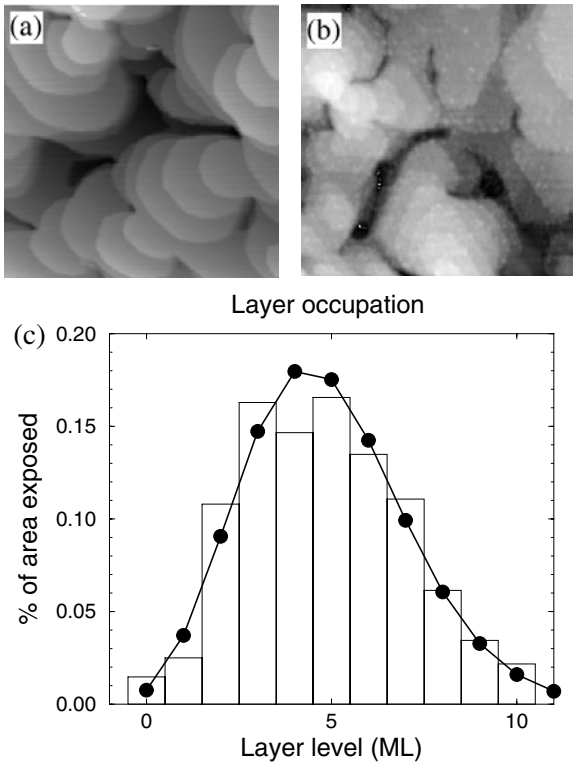

Figure 9. Multilevel growth when interlayer diffusion is suppressed by high ES barriers: (a) 5 ML Cu on Cu(111); (b) 5 ML Co on Cu(111); (c) the experimentally determined distribution of areas exposed on each level in (b) follows Poisson statistics as expected. (These STM images are courtesy of J de la Figuera and J E Prieto.)

in figure 10. During sublimation, atoms detach from the steps (mainly from kink sites) and move into the lower adjacent terrace, where they are confined by the energy barrier at the next edge. An equilibrium density of monomers is thus established. Assuming that the rate of desorption into the vacuum is the same for all terraces, then each step moves backwards with a velocity controlled by the size of the terrace nearby: larger ones can accommodate more adatoms and therefore their ascending steps recede faster, as depicted in figure 10. As a result, any fluctuation in the movement of a train of initially equally spaced steps becomes amplified: wide terraces grow always wider, forcing their steps to catch up with slower ones, forming groups or 'bunches'. The terraces within a bunch are much narrower than their nominal width corresponding to the sample miscut, whereas those separating different bunches are much wider than that value. This phenomenon can have a considerable influence on morphological parameters such as the interfacial roughness in superlattices or the spatial arrangement of nanostructures (quantum wires, dots, etc). On the other hand, step bunching not being an equilibrium configuration, it can be reverted by inverting the conditions that caused it: depositing material onto the surface instead of removing it. In this case, broad terraces receive more adatoms than narrow ones, and thus the lower steps in the bunches advance faster than the others, leaving the group and restoring the equilibrium terrace width.

Kinetic step bunching can appear as a result of the typical procedure for the preparation of metallic surfaces, based on cycles of ion sputtering and high-temperature annealing. During

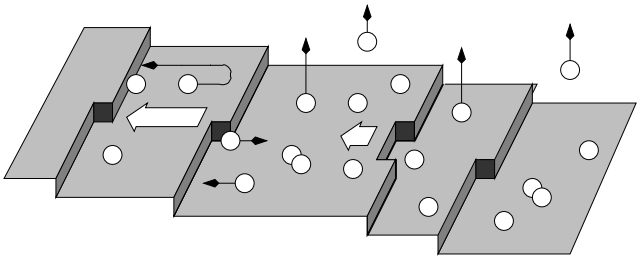

Figure 10. Step recession during sublimation from a surface with interlayer diffusion suppressed by high ES barriers. Step velocity is controlled by the size of the adjacent terrace into which free adatoms are released (from [62]).

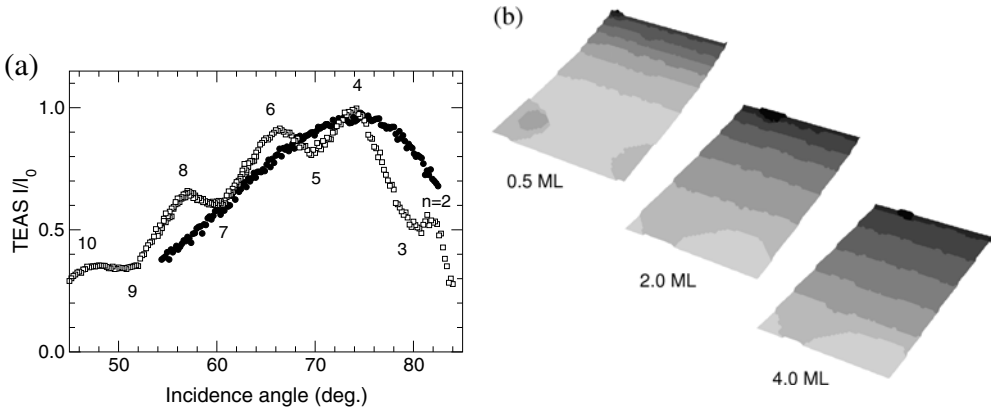

Figure 11. (a) TEAS $\theta - 2\theta$ scans on a Cu(111) surface with step bunches (●), produced by extensive Ar^+ sputtering and high-temperature annealing, and on the same surface with equally spaced steps (□) after deposition of 5 ML of Cu in step-flow mode [107]. (b) Series of snapshots of a kinetic MC simulation showing the break up of a step bunch and the recovery of the equilibrium terrace width upon growth with high atomic mobility.

this latter stage, substantial sublimation can take place, altering the equilibrium distribution of terrace widths as described above. Figure 11(a) shows the results of a TEAS study on Cu(111) [107] that clearly demonstrates this effect. The curve plotted with full circles is a $\theta - 2\theta$ scan measured on the clean Cu surface after extensive annealing. In this kind of experiment, the peak intensity of the specular beam is measured as a function of incidence angle. A modulation of the diffracted intensity is expected as the angle of incidence sweeps across the different interference conditions, with maxima at the angular positions corresponding to in-phase scattering from adjacent terraces and minima when destructive interference leads to cancellation of the diffracted amplitudes at both sides of the steps. The absence of such a structure in the experimental curve implies that the average distance between steps is much larger than the transfer width of the incident He beam. With a detailed analysis of the data one can estimate that the flat areas on this surface are typically 1500 Å wide [62]. The sample miscut was 1°, giving an equilibrium terrace width of 120 Å. This means that the bunches must contain an average of 12 steps.

The inverse process, namely the step debunching caused by deposition, can also be readily demonstrated in this same system. The experimental curve depicted with open squares in figure 11(a) was measured on the same sample reported in the previous paragraph, after having

grown 5 monolayers (ML) of Cu at high temperature in the step-flow mode. Now the maxima and minima caused by interference from adjacent terraces are clearly visible; they have been labelled in the figure according to their order. The same kind of detailed analysis mentioned above [62] shows that the average terrace size on this surface is very close to the nominal one, 120 Å.

Step debunching can be visualized by a simple MC simulation. The snapshots in figure 11(b) show different stages of growth, starting with a bunch of six steps. As a rule of thumb, a more or less equidistant distribution of steps is reached after depositing roughly half as many ML of material as steps are grouped in the bunches. Using this recipe it should be possible to prepare clean, well-ordered surfaces with their equilibrium morphology.

ES barriers also play a leading role in the step-bunching processes that have been shown to result in ripple formation [117, 118] and surface nanopatterning [119] during surface erosion by ion bombardment. Sputtering under normal incidence causes mass transport along the preferential directions for surface diffusion, which are determined by the crystallographic structure of the substrate. When interlayer diffusion is inhibited, the surfaces develop pits [120, 121] or mounds [119] that frequently display a high degree of ordering. This makes the sputtering process a potential candidate for the production of self-organized nanoscale systems, a subject that will be discussed in more detail in section 5.

3.3. Diffusion along steps

It is a widespread belief that the best possible growth mode is ideal LBL with 2D islands nucleated on the terraces and then growing laterally. Unrestricted inter-and intralayer diffusion would ensure that one atomic layer becomes filled before the next one starts to populate. This growth mode can best be monitored through the well-known periodic oscillations of the intensity in diffraction experiments [66–68].

Unfortunately, these conditions are often unfeasible in practice. Leaving aside other limitations (such as reduced diffusion across atomic steps, already dealt with in section 3.2), any realistic substrate must contain a certain density of atomic steps due to the unavoidable surface miscut. Hence, unlimited in-plane diffusion can never be achieved because those steps act as sinks, capturing increasing fractions of adatoms as the latter's mobility grows, and resulting in step-flow growth. This is not undesirable by itself: in this mode the film grows by continuous propagation of the original surface steps. The initial morphology thus replicates itself, with very little or no accumulation of defects. Step-flow growth is therefore a good choice for preparing films of high structural quality, at least in homoepitaxy. In this case fast surface diffusion is a necessary condition to ensure that freshly landed adatoms can rapidly reach the advancing surface steps and stick to them before nucleation of islands on the terraces takes place. However, this is not sufficient to guarantee the smoothness of the growing film. For this latter purpose a large atomic mobility along the edges is also required, in order to wipe out the inhomogeneities that may appear as a consequence of the random arrival of atoms from the terraces [122]. If this is not the case, and atomic diffusion along the edges is slower than on the terraces, then the statistical fluctuations of the step shapes become progressively amplified, giving rise to the appearance of dendrites [123] as illustrated by the kinetic MC simulations presented in figure 12. This phenomenon, called the *Bales–Zangwill effect* [124], is a type of Mullins–Sekerka shape instability [125] and is especially intense on surfaces with poor interlayer diffusion. In these cases, steps advance only by incorporation of atoms arriving from the lower terrace. Protrusions formed randomly along the edges have a higher probability of capturing these diffusing adatoms, and thus grow progressively longer. The cavities left between them become in turn more and more difficult to fill in, since the atoms reaching the

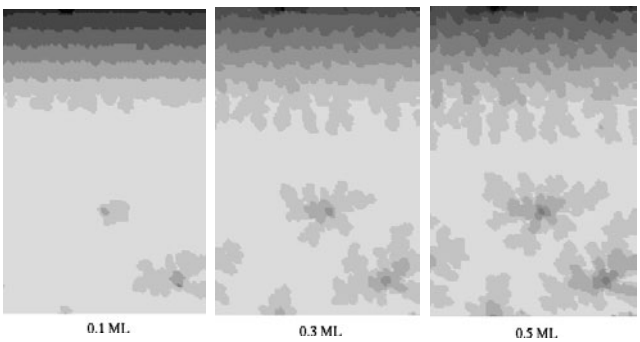

Figure 12. Kinetic MC simulations showing the formation of dendritic edges during growth in the absence of interlayer diffusion and with limited atomic mobility along the steps.

step from its upper side cannot cross the ES barrier.

Once again, compact crystalline faces such as the fcc-(111) fulfil all the requirements for the appearance of rough step flow. There exist abundant studies on those surfaces showing that the activation energy for diffusion along the edges is higher than for free adatoms on flat areas [88, 126–129].

Diffusion along the steps on Cu(111) has been characterized experimentally by means of TEAS [107], taking advantage of the high sensitivity of He atom diffraction for surface defects [62]. The cross section for diffuse scattering from steps, Σ_{st}, is usually measured in length units and represents the extension perpendicular to the edge line over which the surface electronic density is distorted by the presence of the step. He atoms impinging within this area are scattered off the specular direction, and thus they do not contribute to the diffracted intensity measured in a typical TEAS experiment. For Cu(100), Σ_{st} amounts to 12 Å per unit step length [36]. This means that for every step atom 4.7 unit cells become shadowed. The evolution of the step density can then be easily determined from the decrease in the specular TEAS intensity. The amplitude diffracted by the surface is directly proportional to the scattering area. This equals the total surface area minus the fraction covered by the cross sections from the steps:

$$A = A_0\,(1 - \Lambda_{st}\Sigma_{st})$$

where Λ_{st} is the total step length. Taking the square of the amplitude one obtains the diffracted intensity, which is the measurable magnitude:

$$I = |A|^2 = I_0\,(1 - \Lambda_{st}\Sigma_{st})^2$$

Thus the evolution of the surface step density can be derived in a straightforward manner from the measurement:

$$\Lambda_{st} = \frac{1}{\Sigma_{st}}\left[1 - \left(\frac{I}{I_0}\right)^{1/2}\right]. \tag{4}$$

Using a slightly vicinal Cu(111) substrate (miscut angle 1°) step-flow growth can be attained at moderate temperatures, ensuring that diffusion along the edges will be limited. Step roughness in this case is proportional to the total step length; its gradual increase during Cu deposition at different temperatures is revealed by the decaying TEAS specular intensity shown in figure 13(a): here, the total step length as deduced from the measurements by making use of (4) has been represented versus film thickness. The deposition rate was 1.5 ML min^{-1} in all cases. The evolution of the step roughness with time follows a power law behaviour of the type

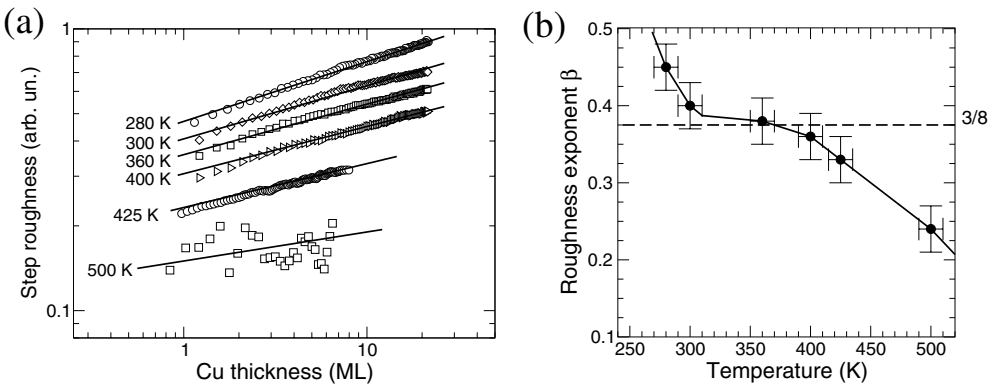

Figure 13. (a) Evolution of step roughness during step-flow growth of Cu on Cu(111), monitored by TEAS. The data show the power-law behaviour typical for kinetic roughening; the full lines are least-squares fits to them. (b) Temperature dependence of the roughness exponent β, indicative of the different regimes of atomic diffusion along the steps (see text). Taken from [107].

$W(L, t) = t^{\beta}$, characteristic for the early stages of kinetic roughening [122, 130, 131]. From fits to the experimental data using this functional form (shown in the figure with full lines), the values of the roughness exponent β can be obtained. They are plotted in figure 13(b) against deposition temperature. Correlating the experimental values of β with the theoretical predictions from different models, many details about edge diffusion can be inferred. For the two limiting cases, namely negligible and unlimited atomic mobility, values of $\beta = 1/2$ and 0 are expected, respectively. The TEAS data demonstrate that the former condition can be reached slightly below 270 K, while the latter seems to lie above 600 K. More interesting are the intermediate regimes. $\beta = 1/4$ corresponds to an atomic mobility just sufficient to reach the nearest local energy minimum [132, 133]; this implies that the atoms can move along the straight step segments and cross corners, becoming immobilized at kink positions. Experimentally, this behaviour is observed at about 500 K. The value $\beta = 3/8$ then appears when corner crossings are forbidden [134], a situation that extends between approximately 300–400 K for Cu(111).

The information furnished by these experiments can be extremely valuable for the preparation of structures of atomic dimensions. The interpretation of the data can be cross-checked with the aid of computer simulations, such as those presented in figure 14. There, the movement of a Cu atom along a kinked atomic step on Cu(111) is monitored in time at different temperatures: (a) 500 K and (b) 700 K. These results were obtained by MD simulations [135] with EAM interatomic potentials [136]. At the lower temperature, the Cu atom moves back and forth along the straight edge, bouncing off the corner; the lower panel shows its trajectory in real time. Different runs like this one proved that, at this temperature, the atoms are not able to cross the corners, in reasonable agreement with the experiments. On the contrary, at 700 K (figure 14(b)) corner crossings take place easily. The first remarkable point is the much higher atomic mobility at this temperature, as demonstrated by the different time scale in the lower panel. Also, the mechanism for corner crossing deserves to be mentioned: upon reaching the kink site, the arriving atom pushes the corner atom away along the step and replaces it, in a sort of one-dimensional exchange equivalent to the already discussed mechanism of interlayer diffusion (see section 2.1.2).

In summary, the different phenomena reviewed in this section confirm the intrinsic complexity of all growth- and diffusion-related processes. Again, these findings call for the development of sophisticated techniques allowing for a precise control of structures and

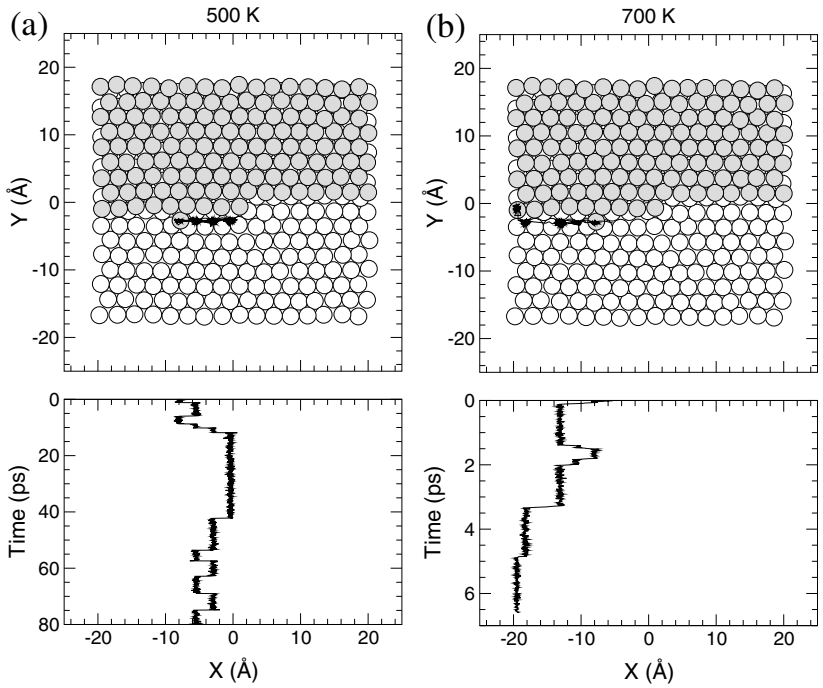

Figure 14. MD simulations of atomic diffusion parallel to an atomic step in Cu(111) at (a) 500 K and (b) 700 K. Corner crossings are only observed in the higher temperature runs. Notice the different time scales in the two lower plots, showing the atoms' trajectories.

morphologies at the atomic scale, as a prerequisite for the successful preparation of artificial nanostructures.

4. Methods of assisted growth

The driving force behind the current intense activity in epitaxial growth and related subjects are the huge economic prospects associated with the perspectives of applications for artificial materials with specially optimized properties. Some of them have already made their way into the markets, such as the solid-state lasers made of semiconductor superlattices or the spin-valve-based reading heads making use of the giant magneto-resistance (GMR) effect. For this reason, the interest of these studies lies not only in learning the details of atomic diffusion, nucleation and epitaxy, but mainly in using this knowledge to find methods to control all those processes and tailor growth as desired. Attempts have been made to stabilize metastable structures by manipulating the systems' kinetics, reducing the atoms' mobility so that they cannot reach their equilibrium configurations. However, this method does not allow us in general to steer growth at will, or to control specific processes. To achieve these goals, more sophisticated procedures are required; some examples will now be presented.

4.1. Surfactants

The term *surfactant* stands for 'surface agent' or 'surface-acting species'. These elements or compounds can accurately be described as catalysts for growth: additives introduced prior

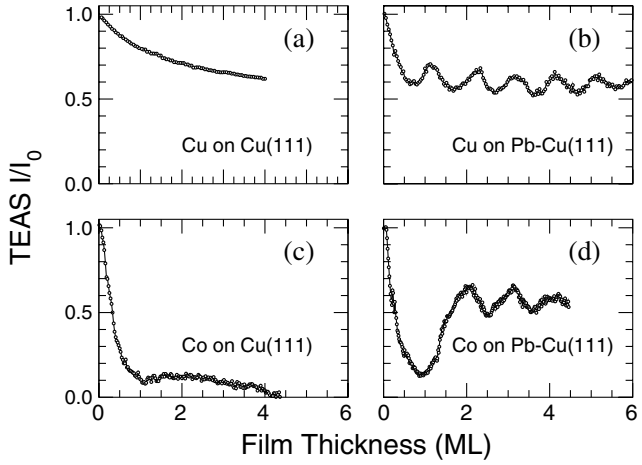

Figure 15. Surfactant-induced LBL growth in systems with high ES barriers and poor interlayer diffusion. Both Cu (a) and Co (c) grow in multilayer mode with negligible interlayer diffusion on Cu(111). In the presence of 1 ML Pb covering the substrate, both materials show LBL growth (panels (b) and (d), respectively).

to starting deposition so that their presence adsorbed on the substrate surface modifies the kinetics and/or energetics of the epitaxial system [137]. Surfactants must segregate rapidly and efficiently to the surface of the growing film, so that they can maintain their activity indefinitely as growth proceeds and, at the same time, no impurities are introduced in the grown layers. Thus, the best candidates for this purpose are materials with low surface energy, which tend to float on top of the epitaxial layer and wet it. A large difference in atomic size between surfactant and deposit also reduces bulk miscibility and favours segregation, as already discussed in section 2.1.1 [24].

Surfactants have long been known in the field of crystal growth [138, 139], but only in recent years have they started to be used for epitaxy. The first experimental observations of growth alterations provoked by additives were done on metallic systems [140, 141]. However, the method reached maturity mostly through work done on semiconductors [142]. From this area, renewed interest has spread back in recent years to the metallic materials. This surge was prompted by observations of significant improvements in the structural quality and magnetic properties of complex heterostructures such as crystalline superlattices [114, 115] or spin valves [143–146].

Surfactants can modify the structure and morphology of epitaxial films in different ways. For instance, one of the main difficulties arising during heteroepitaxy on semiconductors is the accommodation of lattice misfit, due to the stiffness of their covalent bonds. Elements such as Sb or As have been shown to be effective at relieving elastic strain by inducing the formation of misfit dislocations at the interface [147]. For metals, the most significant effects reported so far are the enhancement of LBL growth and the reduction, or even suppression, of stacking fault formation.

4.1.1. Promotion of layer-by-layer growth. This topic has received most of the attention, with abundant studies available in the literature, from both the theoretical and experimental sides. The magnitude of this interest can be well understood in view of the He scattering data presented in figure 15. These graphs show the evolution of the specular TEAS intensity during

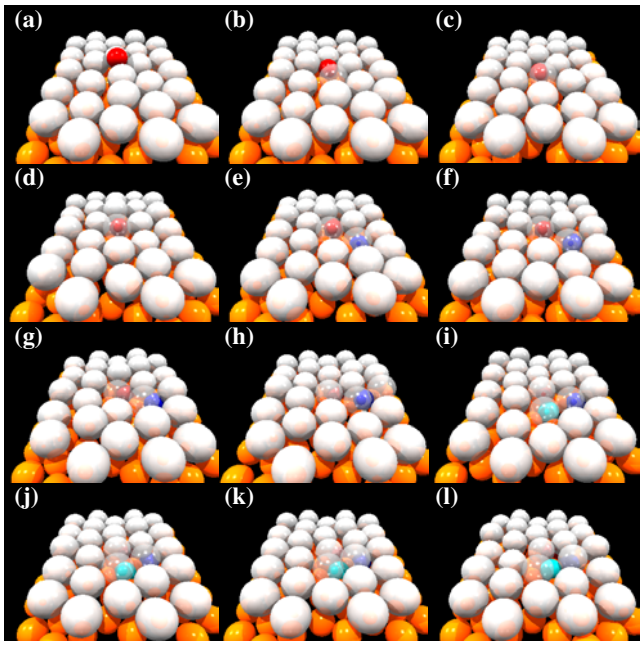

Figure 16. Snapshots of a MC simulation with TB-SMA interatomic potentials and graphically demonstrating atomic diffusion on the presence of a surfactant layer that segregates to the surface upon deposition of the growing material. Immediately after its arrival at the surface, a Cu adatom (red sphere) gets buried below the Pb layer (white spheres) covering the Cu substrate. Below the surfactant, the Cu adatom diffuses by successive site exchanges with other surface atoms (blue, cyan spheres) [82, 167].

the growth of two different materials, namely Cu and Co, on Cu(111). Without surfactant, both Cu (panel (a)) and Co (panel (c)) grow in a multilayer fashion, as demonstrated by the monotonic decrease of the surface reflectivity. The STM images in figures 9(a) and (b) are typical examples of the corresponding growth front morphologies. In the presence of a surfactant, a monolayer of Pb in this case, the situation is radically different: the pronounced oscillations in the intensity of the specular He beam (panels (b) for Cu and (d) for Co) reveal a nearly ideal LBL growth except for the anomalous first monolayer at the Co/Cu interface. Quantitative analysis of the TEAS data, confirmed by STM experiments, has demonstrated that the surfactant induces almost unrestricted interlayer diffusion in both systems, otherwise characterized by the existence of high ES barriers completely suppressing step crossings on their clean surfaces, as already discussed in section 3.2.

These instances of surfactant-induced or enhanced LBL growth are by no means unique. Always restricting ourselves to metallic systems, similar effects have been reported for Ag on Ag(111) with Sb as surfactant [148], Ag on Ag(100) with Sb [149], Cu on Cu(100) with In [150], Co on Cu(110) with O_2 [151] or Cu on Ru(0001) with O_2 [152].

Although the ability of surfactants to induce LBL growth was soon widely recognized, no such agreement existed about the atomic scale mechanisms responsible for that activity. Diverse models were put forward, either on purely theoretical grounds [153–158] or, partially at least, based on experiments [159–162]. However, the majority of these proposals were unsatisfactory: some of them failed to properly account for the experimental observations, and others were too system-specific to explain what seems to be a very general phenomenon.

The likely solution to this puzzle came from a combination of experiments and computer simulations. This work was carried out with a blend of molecular static relaxation and MC simulations in continuous space, using the TB-SMA potentials described above [109]. The great advantage of these computer techniques is their ability to reproduce and visualize intricate processes involving many atoms simultaneously. For the case under study, the relevant sequence of events is summarized in figure 16. In this mosaic of images, constructed from the output of the simulations, one can see (a) how a Cu atom (shown in red) lands on a Pb-covered Cu(111) surface. It then (b)–(d) immediately penetrates across the compact layer of Pb atoms represented with white spheres. Once the Cu atom is sitting at the Cu–Pb interface (e) it cannot diffuse sideways by the hopping method usual on bare Cu(111), because all neighbouring sites are blocked by Pb atoms. With the hopping channel for surface diffusion closed by the presence of the surfactant layer, the only possibility left is atomic exchange. Panels (e)–(h) show a first such event, in which the deposited Cu adatom replaces another one from the substrate (coloured in blue). A second exchange then takes place between the latter and a third substrate atom shown in cyan, (i)–(l). Although these site exchanges seem to be facilitated by the severe distortions induced on the Cu substrate by the Pb overlayer [39], diffusion in the presence of the surfactant seems to be considerably slower than on the very flat, clean Cu(111) surface. As a result, the density of nucleated islands increases by an order of magnitude [163] with the subsequent reduction in their average size and separation. The islands borders also become rougher, with a higher density of kink sites that allow for easier step crossings [135, 164]. This mechanism thus offers a consistent explanation for the surfactant-induced enhancement of interlayer diffusion and is general enough to be applicable to many different systems.

In spite of the obvious difficulties in obtaining a direct experimental confirmation for fast dynamic processes such as those portrayed in figure 16, the overall picture is supported by indirect measurements. For instance, surface x-ray diffraction (S-XRD) data show that the Pb-$p(4 \times 4)$ superstructure formed on Cu(111) remains well ordered during Co and Cu deposition, while the surfactant layer is segregating to the surface [165]. This indicates that the position exchanges between surfactant and deposited atoms are very fast, and that islands of the latter are nucleated below the surfactant layer and not above it. From this it follows that there must exist some significant mobility of the growing species at the Pb–Cu(111) interface. Additional TEAS and STM experiments showed that those islands, covered by the surfactant layer, can be dissolved by gentle annealing [109], the released material being able to diffuse (most likely below the Pb overlayer and by the exchange mechanism depicted in figure 16) away from its original nucleation sites to reach the surface steps.

Several consequences derive from this model. First, the effect is of local nature: the surface must be completely covered by the surfactant because on uncovered patches diffusion and nucleation take place as on the bare substrate. Figure 17 provides an experimental confirmation to this statement: it displays a series of Cu depositions monitored with TEAS and performed on Cu(111) precovered with different amounts of Pb. The surfactant coverages are indicated in text on each graph and also graphically on the central panel, which shows them on the TEAS uptake curve for Pb on Cu(111), already described in detail in section 2.1.1. Clearly, the oscillations of the diffracted intensity characteristic of LBL growth only appear close to or above monolayer coverage.

Another implication has to do with the quality of the interfaces formed during surfactant-assisted growth. As long as diffusion of the growing species takes place by exchange, there will be an unavoidable amount of intermixing, affecting at least two atomic layers, the uppermost one from the substrate and the first one in the deposit. Whether this fact is acceptable or not in trade for an improved morphology and film continuity derived from the use of the surfactant will depend on each particular case and on the specific properties sought from the grown material.

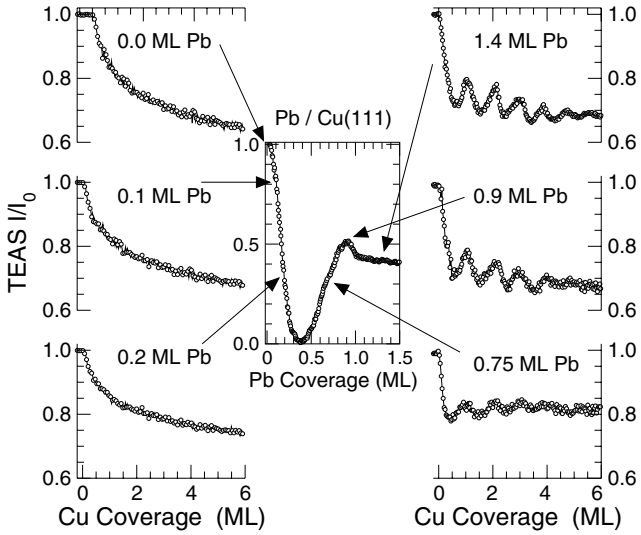

Figure 17. Series of Cu depositions on Cu(111) covered with different amounts of Pb. The oscillations in the specular TEAS intensity indicate that the optimum surfactant coverage is a full monolayer.

4.1.2. Suppression of stacking fault formation and twinning. A second, important practical application of surfactants is their ability to influence the crystalline structure of the epitaxial deposits. This aspect has been explored in less detail than the former, but still there exists firm experimental evidence about it. The first observation reported the suppression of twinning on fcc-Cu capping layers deposited on top of Co films grown on Cu(111) with a monolayer of Pb acting as surfactant [111]. This effect was first attributed to a delayed fcc-to-hcp transition in the Co layer. Nevertheless, it was later found that the same surfactant was able to reduce by an order of magnitude the probability of Cu atoms nucleating stacking-faulted islands on clean Cu(111) at room temperature [165].

Figure 18 shows S-XRD scans measured along the $\{10\}$ crystal truncation rods (CTRs), after growing Cu films at room temperature on a Cu(111) substrate. In this type of experiment, the diffracted intensity is measured as a function of perpendicular momentum transfer, providing information on the stacking sequence of the sample [107]. The film represented with filled circles was grown on the clean Cu(111) surface, whereas the one depicted with open squares was deposited on the same substrate covered with a monolayer of Pb. The full lines are kinematic fits to the data; they were obtained using appropriate structural models for the respective overlayers. The curves have been displaced vertically for the sake of clarity. The intense peaks noticeable at $l = 1$ and 4 are bulk Bragg reflections corresponding to the fcc-(111) orientation. The feature developing at $l = 2$ signals the appearance of twinned crystallites and is significantly reduced when the surfactant is present (notice the logarithmic intensity scale). The fits to the data indicate that the probability to form a stacking fault at room temperature on clean Cu(111) is $\sim$20%, whereas with Pb it decreases to a mere 2%.

A similar result has been reported using In as a surfactant, also during the growth of Cu on Cu(111) [166]. Thus, it seems to be an intrinsic effect. Computer simulations and total energy calculations with the TB-SMA interatomic potentials mentioned above have shown that the distortions induced on the uppermost substrate layers by the presence of the adsorbed surfactant increase the energy asymmetry between the different fcc and hcp adsorption sites within the

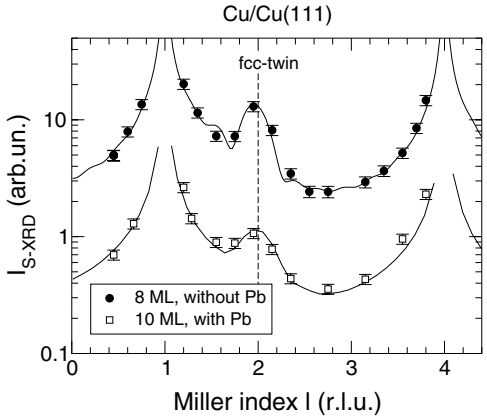

Figure 18. S-XRD scans in perpendicular momentum transfer ('rod scans') obtained after growing two films of Cu on Cu(111) at room temperature, one without surfactant (●) and another in the presence of a monolayer of Pb (□). The peak at $l = 2$ signals the appearance of twinned fcc-(111) crystallites, being much reduced by the surfactant (notice the logarithmic intensity scale). The full lines are fits to the data. The curves have been shifted vertically for clarity.

reconstructed unit cell. While the stacking fault energy on clean Cu(111) is estimated to be about 7–10 meV/atom [107], on the Pb-covered surface the average energy difference rises to $\langle E_{\mathrm{hcp}} - E_{\mathrm{fcc}} \rangle = 0.10 \pm 0.03$ meV per atom [167]. Although this result may not be generally applicable to other combinations of surfactant and substrate, the atomistic mechanism seems general enough to guarantee that there will exist other examples. It also seems conceivable that other surfactants may favour the formation of stacking faults or the transition to a different crystallographic phase. More work is needed to explore the possibilities of this method.

4.2. Codeposition

Very often, materials designed for specific applications must reach some minimum dimensions in order to perform their functions. This requirement may arise either from fundamental reasons (like, for instance, showing non-zero remanence at finite temperature in low-dimensional magnetic materials [168, 169]) or else be due to practical criteria, in order to maximize the system's response or increase the signal-to-noise ratio, as is the case for magneto-optic materials for data storage and retrieval.

Superlattices can be considered a special case. The constitution of these heterostructures, organized as a sequence of alternating layers of two or more components, serves several purposes. It allows for a considerable increase in the total thickness of material that can be piled up while at the same time maintaining its low-dimensional character, at least along the growth direction. The chemical periodicity introduced generates novel properties that can be tuned through its period length, among others. Finally, the rupture of symmetry caused by the presence of numerous interfaces also enhances important characteristics such as magnetic anisotropy, magneto-resistance or electron confinement.

All the enunciated purposes require the maintenance of structural coherence during growth, in order to minimize the accumulation of defects and ensure the quality of interfaces. One of the main obstacles that must be overcome to reach those goals is the natural tendency of the growing materials to adopt their equilibrium lattice constant and crystalline phase. As pointed out in section 3.2, the transition to bulk structure usually takes place over an extended range

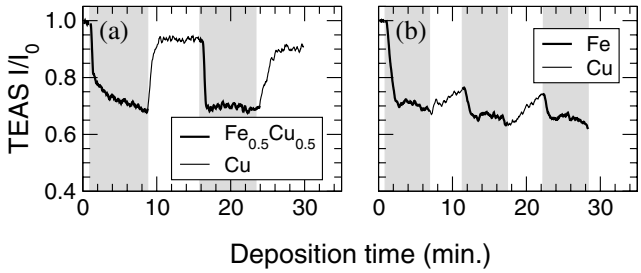

Figure 19. Growth of superlattices of Fe and Cu, monitored by TEAS and using 1 ML of Pb as surfactant. (a) When Fe and Cu are codeposited, the fcc structure dictated by the Cu(111) substrate is preserved, and the spacer layers of Cu reach a high reflectivity, indicating good structural quality. (b) In layers of pure Fe the transition to bcc breaks the sample's structural coherence, producing very rough interfaces and a continuous accumulation of defects.

of thicknesses, thereby producing inhomogeneous, discontinuous films. A possible way to circumvent this limitation might be to codeposit a second material, which, depending on the relative concentrations, may act either as a dopant or as an embedding matrix and impose a particular structure on the first component.

This method has been known for a long time, having been used mainly to produce granular materials [170], frequently by annealing metastable samples grown either by rapid cooling or multilayers of immiscible elements. Lately, the progress reached both in growth methods and characterization techniques, together with the observation of interesting properties such as GMR has called back attention to this kind of system. The codeposition method, combined with the use of surfactants, has been tested recently on the Fe–Cu/Cu(111) and Co–Cu/Cu(111) systems. The growth of fcc-Fe with a lattice constant slightly increased with respect to its bulk value is particularly interesting because the existence of a high-spin phase has been predicted [171]. In fact, ultrathin Fe films (up to 3–4 ML) with enhanced magnetic moments have been realized both on Cu(100) [172] and on Cu(111) [173] using pulsed laser deposition. The extremely high evaporation rates attained with this method help stabilize metastable structures through kinetic constraints. Nevertheless, with increasing thickness the Fe films always transform to the bulk bcc phase. Tackling the problem from a different side, the feasibility of stabilizing precipitates of γ-iron within a Cu matrix is well known [174], although in this case the Fe particles were found to be antiferromagnetic [175].

There is thus a clear interest in finding methods to produce fcc-Fe with controlled magnetic properties. The codeposition approach has been applied recently in an attempt to grow (Fe/Cu) superlattices with (111) orientation [176], using a Cu single crystal as substrate and 1 ML of Pb as surfactant. The preliminary results of this experiment are summarized by the TEAS data presented in figure 19. Panel (a) displays the evolution of the surface reflectivity during the growth at RT of several periods consisting of a mixed Fe–Cu film (thicker line within the shaded area) with a total thickness of approximately 12 ML and a 50–50% composition, and a second layer with 6 ML of pure Cu (thinner line over the white background). During the deposition of the latter, the specular TEAS intensity rises close to its initial value, indicating that the surface is nearly as perfect as before starting growth. Such a low rate of defect accumulation should allow us to stack a large number of periods, in order to increase the magnetic signal and also to fully exploit the special properties derived from the superlattice periodicity. A qualitative look at low energy electron diffraction (LEED) I–V measurements on this sample reveals that the film structure is fcc-like, although a more detailed analysis is needed to determine whether it is distorted or not. In any case, the presence of bcc-Fe can be ruled out. The films also show

magnetic remanence at RT as determined from SMOKE (surface magneto-optic Kerr effect) measurements; further work is in progress to characterize in detail the magnetic properties of these bimetallic films. The structural improvements derived from the codeposition method can be fully appreciated by comparing the former results with those depicted in figure 19(b), which show a similar TEAS experiment monitoring the specular intensity diffracted while growing a superlattice made up of pure Fe films 5 ML thick alternating with 4 ML of Cu. Clearly, the surface recovery during the growth of the Cu spacers is not enough to heal the disorder accumulated within the Fe layers (where LEED shows that the transition to bcc has already started) and the sample morphology rapid and continuously degrades.

Let us now briefly discuss another representative case. Co/Cu superlattices grown by sputtering have for some time held the record for magneto-resistance, reaching values in excess of 65% at RT [177]. Similar structures prepared by thermal deposition failed repeatedly to display an analogous behaviour [141, 178]; it was later demonstrated that such a poor performance was related to the existence of discontinuities or '*pinholes*' providing direct contacts between consecutive magnetic layers and thus forcing them to be ferromagnetically aligned [52]. The origin of these defects can be traced back to the appearance of crystallites of hcp-Co and twins of fcc-Cu within the respective layers. Using a surfactant (Pb) to assist growth proved to be useful to reduce the amount of twinning in the Cu [111], thereby enabling the appearance of complete antiferromagnetic alignment of the Co layers [180]. However, the presence of the surfactant is not enough to prevent the latter from adopting the hcp structure [163]. The existence of this transition imposes strict limits on the thickness of the Co layers that can be used to prepare superlattices of good structural quality. Nevertheless, these limits can be overcome by using the codeposition approach: figure 20 shows XRD reflectivity scans measured on a $\{[Co_{0.5}Cu_{0.5}]_{14\,ML}/[Cu]_{7\,ML}\}_{\times 22}/Cu(111)$ superlattice grown at RT by this procedure, also using 1 ML Pb as surfactant. The large number of intense satellite peaks visible both at low (panel (a)) and high angle (panel (b)) indicates that the superlattice periodicity is well defined and the interfaces are sharp. Kiessig fringes can also be observed (see the inset in figure 20 (b)), implying that the whole film is homogeneous over long lateral distances. The x-ray measurement did not detect any traces of hcp-Co within the sample, although the amount of Co within each mixed layer exceeds the typical values (3–7 ML) for which the fcc-to-hcp transition has been observed [163, 165]. Magnetic measurements performed on this superlattice [115] have shown that it is ferromagnetic at RT, with a reduced coercivity and a large polarizability as compared with samples containing layers of pure Co.

The examples described in this section aim to demonstrate the usefulness of the codeposition method to create metastable epitaxial structures, especially when combined with other strategies to assist growth such as the use of surfactants. Hopefully more work will be devoted in the future to explore and widen the capabilities of this procedure.

4.2.1. Other methods of assisted growth. Before closing this section, some space should be devoted to mention other methods to assist or modify growth that have been reported in the literature. Gentle, pulsed bombardment of the surface with low energy ions has been employed with the aim of controlling nucleation [181]. The point defects created on the surface by the impinging ions act as preferential nucleation centres, inducing the formation of a higher density of islands at specific stages of growth, right after completion of every atomic layer. A similar effect can be obtained by modulating the supersaturation of monomers on the surface, either by reducing the sample temperature or by increasing the deposition rate at the appropriate moments [181, 182]. In all cases, these strategies try to favour the appearance of single-atomic-height islands when the surface is nearly ideally flat, and then reduce the probability of nucleation while those islands are growing laterally, in order to prevent higher atomic levels

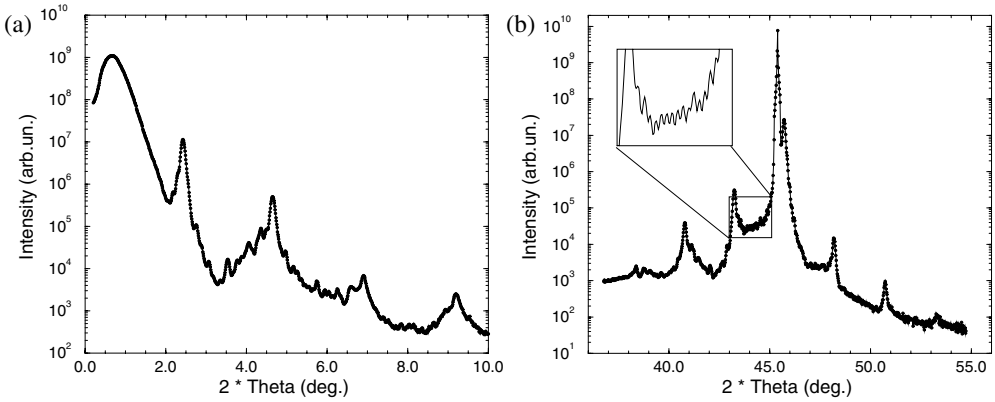

Figure 20. X-ray reflectivity measurements on a $\{[Co_{0.5}Cu_{0.5}]/Cu\}_{\times 22}/Cu(111)$ superlattice grown by codeposition and using one surfactant ML of Pb. The satellite diffracted peaks visible at both low (a) and high (b) incidence angle indicate well-defined interfaces and good crystallinity. Kiessig fringes are also observed (shown in detail within the inset in (b)), implying that the sample thickness is homogeneous over a large extent (from [114]).

from starting to populate. These techniques have succeeded to some extent in inducing LBL growth in systems like Cu/Cu(111) that usually grow in multilayer mode [181, 183].

For systems that do not grow spontaneously LBL, low temperature deposition can induce 2D growth through kinetic constraints on the adatoms' diffusivity. For instance, Pb grows Stranski–Krastanov on Cu(111) at room temperature, but switches to Frank–van der Merwe at low temperature [184]. This is obviously a metastable state caused by the reduced mobility of the deposited adatoms. This effect is also useful to prevent or at least reduce interdiffusion in those cases for which mixing takes place by the island instability mechanism described in section 2.2. Growing at low temperature or using very high deposition rates (as with pulsed laser deposition [60]) results in the formation of many small islands with dendritic shapes due to diffusion-limited aggregation. These ramified structures seem to relieve the misfit strain efficiently, and thus no surface etching or double-atomic-layer growth is detected [185, 186]. The main drawback of this technique is the general reduction of all thermally activated processes, including atomic diffusion, with the subsequent increase of surface or interface roughness.

5. Self-assembly and self-organization

This review could not finish without including at least a brief mention of a number of recent reports showing the appearance of spontaneously ordered structures of atomic size on metallic systems. Self-assembly and self-organization are promising bottom-up approaches towards finding efficient production methods to reach the ultimate miniaturization. Spontaneous long-range ordering usually results from an interplay between attractive and repulsive interactions. This can be the case with several of the phenomena discussed in this paper, such as the different bonding energies in multicomponent systems or the tendency to relieve accumulated elastic strain competing against the loss of structural coherence between substrate and overlayer.

While matching two different materials at the interfaces of heteroepitaxial systems conveys a variety of problems, as already described in the previous sections, combining them in bimetallic films can offer enhanced possibilities for manipulation. A study by Hwang [187] showed that the codeposition of two immiscible metals can result, under appropriate conditions,

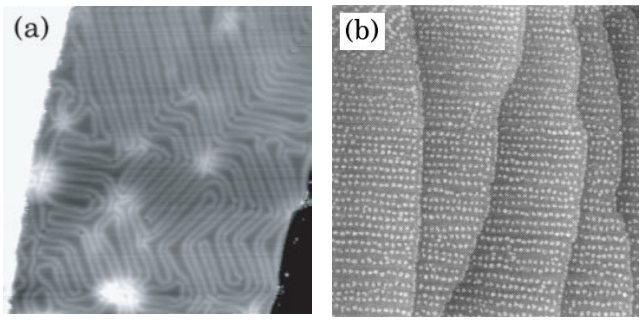

Figure 21. (a) Surface reconstruction of a 2 ML thick Cu film on Ru(0001). The brighter lines are slightly elevated boundaries separating regions with fcc and hcp stacking, which appear as the Cu film tries to relieve its misfit strain. The corners in these ridges are specially reactive positions, potentially providing sites for self-organized preferential nucleation [192]. (b) Array of well-ordered Co clusters grown on Au(111). This STM image has 3000× 3000 Å^2 islands nucleated on the kinks of the $22 \times \sqrt{3}$ surface reconstruction (taken from [169]).

in phase separation of the components. This fact has been taken advantage of to produce self-ordered structures such as lateral superlattices of Co–Ag and Fe–Ag on Mo(110) surfaces [188] or atomic wires of Ag–Co by decorating the atomic steps on vicinal Pt(111) [189].

Another interesting approach relies on taking advantage of the strain relaxation processes that must unavoidably occur at some point during heteroepitaxial growth. Traditionally, the accommodation of lattice misfit has represented one of the toughest problems to solve for the obtention of continuous, ultrathin films of good structural quality. It is thus rather paradoxical that conveniently engineered misfit strain now provides an efficient pathway to produce large-scale arrangements of self-assembled or self-organized structures of nanometric size. Most of the earlier research on this topic has been concentrated on semiconductor materials, on which impressive progress has been achieved [190, 191]. Nevertheless, the recent appearance of a number of promising results on metallic systems has caused a surge of investigations in this area.

As an example, figure 21(a) presents a STM image of 700 Å on each side showing the herringbone-type reconstruction of a 2 ML thick Cu film grown on Ru(0001) [192]. The bright lines forming the zig-zag structure are domain boundaries separating regions in the second Cu monolayer with fcc and hcp stacking. The atoms within these boundaries are higher than the rest because they occupy near-bridge positions. This is the same kind of reconstruction that gives rise to the $22 \times \sqrt{3}$ superstructure on Au(111). The zig-zag pattern allows for an efficient release of the strain in all directions within the surface layer and can be prepared with a high degree of ordering over extended areas. The kinks in the elevated ridges provide preferential nucleation sites for material deposited on top of these layers. Figure 21(b) demonstrates how this type of surface can be successfully used as a template for the growth of well-ordered arrays of nanoparticles: in this case, Co clusters of approximately 3 nm diameter nucleated at the corners of the reconstruction on a Au(111) substrate [169]. The regularity in the spatial distribution of the islands also results in a high uniformity of sizes, since the capture areas surrounding each cluster are very nearly equal [193].

Heterogeneous nucleation is not the only way to obtain uniform epitaxial structures. Under conditions of relatively high atomic mobility, Co grows on Ru(0001) in the Stranski–Krastanov mode, with a single wetting Co ML followed by 3D islands to relax the strain caused by the ∼7.3% lattice misfit. The islands formed during this process display rather well-defined

distributions of sizes and other morphological features [194], and can therefore be considered an example of self-assembled nanostructures. Somewhat similar results have been obtained on other systems, such as Gd/W(110) [195] or Co/Al_2O_3 [196].

In conclusion, these phenomena of self-assembly and self-organization open vast new possibilities of research in the subject of low-dimensional metallic structures. This is an area that will certainly attract intense attention in the very next future.

6. Summary

Research on metallic heterostructures has been plagued with difficulties whose origin can be traced back to very basic processes at the atomic level. In this paper we have reviewed different aspects of the epitaxial growth of metals from an atomistic point of view, emphasizing those which appear to be more ubiquitous when considering a wide variety of systems and at the same time to play a most significant role on determining the final samples' morphology and structure, and hence also their properties and performance. Representative examples have also been provided based on recent theoretical and experimental work. It has been shown that strain relaxation in lattice-misfitting systems can lead not only to the well-known formation of dislocations, but it can also enhance interfacial alloying of even bulk-immiscible species. Fine details of atomic diffusion also have a profound influence on growth quality: for instance, the existence of energy barriers hindering interlayer mass transport (ES barriers) can result in step bunching on clean surfaces and provoke a substantial build-up of surface and step roughness with increasing film thickness. Paradoxical as it may appear, in these cases slower in-plane diffusion as on the relatively open fcc-(100) faces leads to a better LBL growth than high atomic mobility, as is usually the case for unreconstructed fcc-(111) surfaces. We have also discussed several special growth methods that have been successfully employed to solve some of the above-mentioned problems for the growth of metallic heterostructures. Finally, some promising approaches to the preparation of self-assembled and self-organized nanoscale systems have also been briefly examined.

Acknowledgments

We would like to express our gratitude to all our collaborators who took part over the years in the different parts of the work reviewed in this paper; among them are A Sánchez, J Ibáñez, A Cebollada, J M Gallego, S Ferrer, J de la Figuera, J E Prieto, A L Vázquez de Parga, C Ocal, J M García, O Sánchez, R Otero, J E Ortega, J Álvarez, M J Capitán, V Cros, J Camarero, D Farías, J Ferrón, C Slutzky, L Gómez, C M Schneider, W Kuch, J Kirschner and K Heinz. Fruitful discussions with Professor I Markov are also sincerely acknowledged. This work has been supported by the MCyT through Project No BFM2001-0174.

References

[1] Esaki L and Tsu R 1970 *IBM J. Res. Dev.* **14** 61
[2] Yoffe A D 2001 *Adv. Phys.* **50** 1
[3] Gibbs J W 1878 *Trans. Conn. Acad.* **3** 343
[4] Kossel W 1927 *Nachr. Ges. Wiss. Göttingen, Math.-Phys.* K **1** 135
[5] Stranski I N 1928 *Z. Phys. Chem.* **36** 259
[6] Burton W K, Cabrera N and Frank F C 1951 *Phil. Trans. R. Soc.* **243** 299
[7] Frank F C and van der Merwe J H 1949 *Proc. R. Soc.* A **198** 205
Frank F C and van der Merwe J H 1949 *Proc. R. Soc.* A **198** 216
Frank F C and van der Merwe J H 1949 *Proc. R. Soc.* A **200** 125

[8] Binnig G, Rohrer H, Gerber C and Weibel E 1982 *Phys. Rev. Lett.* **49** 57
[9] Rodriguez J A and Goodman D W 1992 *Science* **257** 897
[10] Besenbacher F, Pleth Nielsen L and Sprunger P T 1997 Surface alloying in heteroepitaxial metal-on-metal growth *The Chemical Physics of Solid Surfaces and Heterogeneous Catalysis, vol 8, Growth and Properties of Ultrathin Epitaxial Layers* (Amsterdam: Elsevier) p 207
[11] Christensen A, Ruban A V, Stoltze P, Jacobsen K W, Skriver H L, Nørskov J K and Besenbacher F 1997 *Phys. Rev.* B **56** 5822
[12] Feibelman P J 1990 *Phys. Rev. Lett.* **65** 729
[13] Kellogg G L and Feibelman P J 1990 *Phys. Rev. Lett.* **64** 3143
[14] Flores T, Junghans S and Wuttig M 1997 *Surf. Sci.* **371** 14
[15] Pope T D, Anderson G W, Griffiths K, Norton P R and Graham G W 1991 *Phys. Rev.* B **44** 11 518
[16] Schieffer P, Tuilier M-H, Hanf M C, Krembel C, Gewinner G, Chandesris D and Magnan H 1998 *Phys. Rev.* B **57** 15 507
[17] Fassbender J, Allenspach R and Dürig U 1997 *Surf. Sci. Lett.* **383** L742
[18] Nouvertné F, May U, Bamming M, Rampe A, Korte U, Güntherodt G, Pentcheva R and Scheffler M 1999 *Phys. Rev.* B **60** 14 382
[19] Sander D 1999 *Rep. Prog. Phys.* **62** 809
[20] Miedema A R 1978 *Z. Metall.* **69** 455
[21] Miedema A R, de Châtel A F and de Boer F R 1980 *Physica* B & C **100** 1
[22] Chelikowsky J R 1984 *Surf. Sci.* **139** L197
[23] Tersoff J 1995 *Phys. Rev. Lett.* **74** 434
[24] Haasen P 1996 *Physical Metallurgy* (Cambridge: Cambridge University Press) p 142
[25] Pleth Nielsen L, Besenbacher F, Stensgaard I, Lægsgaard E, Engdahl C, Stoltze P, Jacobsen K W and Nørskov J K 1993 *Phys. Rev. Lett.* **71** 754
[26] Röder H, Schuster R, Brune H and Kern K 1993 *Phys. Rev. Lett.* **71** 2086
[27] Altman E I and Colton R J 1994 *Surf. Sci.* **304** L400
[28] Meyer J A and Behm R J 1995 *Surf. Sci.* **322** L275
[29] Sprunger P T, Lægsgaard E and Besenbacher F 1996 *Phys. Rev.* B **54** 8163
[30] Stranski I N and Krastanov L 1938 *Sitzungsber. Akad. Wissenschaft Wien* **146** 797
[31] Henrion J and Rhead G E 1972 *Surf. Sci.* **29** 20
[32] de Beauvois C, Girard Y, Pérard C, Croset B and Mutaftschiev B 1996 *Surf. Sci.* **367** 129
[33] Otero R, Vázquez de Parga A L and Miranda R 2002 *Phys. Rev.* B **66** 115401
[34] Poelsema B and Comsa G 1989 *Scattering of Thermal Energy Atoms (Springer Tracts in Modern Physics vol 115)* (Berlin: Springer)
[35] Comsa G and Poelsema B 1985 *Appl. Phys.* A **38** 153
[36] Sánchez A, Ibáñez J, Miranda R and Ferrer S 1987 *J. Appl. Phys.* **61** 1239
[37] Sánchez A and Ferrer S 1987 *Surf. Sci.* **187** L857
[38] Nagl C, Haller O, Platzgummer E, Schmid M and Varga P 1994 *Surf. Sci.* **321** 237
[39] Müller S, Prieto J E, Rath C, Hammer L, Miranda R and Heinz K 2001 *J. Phys.: Condens. Matter* **13** 1793
[40] Somorjai G A 1994 *Introduction to Surface Chemistry and Catalysis* (New York: Wiley)
[41] Yu B D and Scheffler M 1996 *Phys. Rev. Lett.* **77** 1095
[42] Lundgren E, Stanka B, Leonardelli G, Schmid M and Varga P 1999 *Phys. Rev. Lett.* **82** 5068
[43] Ferrón J 2001 private communication
[44] Raeker T J and DePristo A E 1992 *J. Vac. Sci. Technol.* A **10** 2396
[45] Gómez L, Slutzky C, Ferrón J, de la Figuera J, Camarero J, Vázquez de Parga A L, de Miguel J J and Miranda R 2000 *Phys. Rev. Lett.* **84** 4397
[46] Zhang L P, Kuhn M and Diebold U 1997 *Surf. Sci.* **371** 223
[47] Shen J, Klaua M, Ohresser P, Jenniches H, Barthel J, Mohan Ch V and Kirschner J 1997 *Phys. Rev.* B **56** 11 134
[48] Farías D, Braun K-F, Fölsch S, Meyer G and Rieder K-H 2000 *Surf. Sci.* **470** L93
[49] de la Figuera J, Huerta-Garnica M A, Prieto J E, Ocal C and Miranda R 1995 *Appl. Phys. Lett.* **60** 1006
[50] Hugenschmidt M B, Hitzke A and Behm R J 1996 *Phys. Rev. Lett.* **76** 2535
[51] Rabe A, Memmel N, Steltenpohl A and Fauster T 1994 *Phys. Rev. Lett.* **73** 2728
[52] de la Figuera J, Prieto J E, Ocal C and Miranda R 1993 *Phys. Rev.* B **47** 13 043
de la Figuera J, Prieto J E, Ocal C and Miranda R 1996 *Surf. Sci.* **349** L139
[53] See, for instance,
Materials Theory, Simulations and Parallel Algorithms (MRS Mater. Res. Soc. Symp. Proc. vol 408) (Pittsburg, PA: Materials Research Society)

[54] Cleri F and Rosato V 1993 *Phys. Rev.* B **48** 22
[55] Gómez L and Diep H T 1995 *Phys. Rev. Lett.* **74** 1807
[56] Gómez L, Diep H T and Dobry A 1997 *Phys. Rev.* B **55** 6265
[57] Khalil J, Bozzolo G, Farías D, Vázquez de Parga A L, de Miguel J J and Miranda R 2002 *Current Issues in Heteroepitaxial Growth-Stress Relaxation and Self Assembly (Mater. Res. Soc. Symp. Proc. vol 696)* ed E A Stach, E H Chason, R Hull and S D Baderer (Pittsburg, PA: Materials Research Society) p 265
[58] Li H and Tonner B P 1990 *Surf. Sci.* **237** 141
[59] Schmid A K and Kirschner J 1992 *Ultramicroscopy* **42–44** 483
[60] Jenniches H, Klaua M, Höche H and Kirschner J 1996 *Appl. Phys. Lett.* **69** 3339
[61] Voigtländer B, Meyer G and Amer N M 1991 *Phys. Rev.* B **44** 10 354
[62] de Miguel J J, Camarero J and Miranda R 2002 *J. Phys.: Condens. Matter* **14** 6155
[63] de Miguel J J, Cebollada A, Gallego J M, Ferrer S, Miranda R, Schneider C M, Bressler P, Garbe J, Bethke K and Kirschner J 1989 *Surf. Sci.* **211/212** 732
[64] de Miguel J J, Cebollada A, Gallego J M and Miranda R 1990 *Kinetics of Ordering and Growth at Surfaces (NATO ASI Series B vol 239)* (New York: Plenum) p 483
[65] de Miguel J J, Cebollada A, Gallego J M, Miranda R, Schneider C M, Schuster P and Kirschner J 1991 *J. Magn. Magn. Mater.* **93** 1
[66] Gronwald K D and Henzler M 1982 *Surf. Sci.* **117** 180
[67] Neave J H, Joyce B A, Dobson P J and Norton N 1983 *Appl. Phys.* A **31** 1
[68] Gómez L J, Bourgeal S, Ibáñez J and Salmerón M 1985 *Phys. Rev.* B **31** 2551
[69] de Miguel J J, Cebollada A, Gallego J M, Ferrón J and Ferrer S 1988 *J. Cryst. Growth* **88** 442
[70] Feibelman P J, Kellogg G L and Nelson J S 1994 *Phys. Rev.* B **49** 10 548
Boisvert G, Lewis L J, Puska M J and Nieminen R M 1995 *Phys. Rev.* B **52** 9078
Stumpf R and Scheffler M 1995 *Phys. Rev. Lett.* **72** 254
[71] For a detailed comparison between different experimental techniques and their capabilities applied to surface diffusion measurements, see
Tringides M C 1997 *Surface Diffusion: Atomistic and Collective Processes (NATO ASI Series B vol 360)* (New York: Plenum) p 1
For references to actual experiments on surface diffusion, see
Ehrlich G 1997 *Surface Diffusion: Atomistic and Collective Processes (NATO ASI Series B vol 360)* (New York: Plenum) p 23
[72] Cowell-Senft D and Ehrlich G 1995 *Phys. Rev. Lett.* **74** 294
[73] Senft D C 1996 *Appl. Surf. Sci.* **94/95** 231
[74] Ferrando R, Spadacini R and Tommei G E 1993 *Phys. Rev.* E **48** 2437
[75] Bassett D W 1983 *Surface Mobilities on Solid Materials* (New York: Plenum) p 63
[76] Binder K and Stauffer D 1974 *Phys. Rev. Lett.* **33** 1006
[77] Voter A F 1986 *Phys. Rev.* B **34** 6819
[78] Bogicevic A, Ovesson S, Hyldgaard P, Lundqvist B I, Brune H and Jennison D R 2000 *Phys. Rev. Lett.* **85** 1910
[79] Repp J, Moresco F, Meyer G, Rieder K-H, Hyldgaard P and Persson M 2000 *Phys. Rev. Lett.* **85** 2981
[80] Ehrlich G 1994 *Surf. Sci.* **299/300** 628
[81] Gomer R 1990 *Rep. Prog. Phys.* **53** 917
Kellogg G L 1994 *Surf. Sci. Rep.* **21** 1
[82] Computer simulations courtesy of Gómez L and Ferrón J
[83] Yu B D and Scheffler M 1997 *Phys. Rev.* B **56** R15 569
[84] Roşu M F, Laurens C R, Falepin A, James M A, Langelaar M H, Pleiter F, Rogojanu O C and Niesen L 1998 *Phys. Rev. Lett.* **81** 4680
[85] Chen C and Tsong T T 1990 *Phys. Rev. Lett.* **64** 3147
[86] Bassett D W and Webber P R 1978 *Surf. Sci.* **70** 520
[87] Wrigley J D and Ehrlich G 1980 *Phys. Rev. Lett.* **44** 661
[88] Karimi M, Tomkowski T, Vidali G and Biham O 1995 *Phys. Rev.* B **52** 5364
[89] Liu C L 1994 *Surf. Sci.* **316** 294
[90] Liu C L, Cohen J M, Adams J B and Voter A F 1991 *Surf. Sci.* **253** 334
[91] Tian Z J and Rahman T S 1993 *Phys. Rev.* B **47** 9751
[92] Sanders D E and DePristo A E 1992 *Surf. Sci.* **260** 116
[93] Perkins L S and DePristo A E 1993 *Surf. Sci.* **294** 67
[94] Hansen L, Stoltze P, Jacobsen K W and Nørskov J K 1991 *Phys. Rev.* B **44** 6523
[95] Trushin O S, Kokko K, Salo P T, Hergert W and Kotrla M 1997 *Phys. Rev.* B **56** 12135

[96] Breeman M and Boerma D O 1992 *Surf. Sci.* **269/270** 224
[97] Ernst H J, Fabre F and Lapujoulade J 1992 *Phys. Rev.* B **46** 1929
[98] Dürr H, Wendelken J F and Zuo J-K 1995 *Surf. Sci. Lett.* **328** L527
[99] Madhukar A 1983 *Surf. Sci.* **132** 344
[100] Lapujoulade J 1981 *Surf. Sci.* **108** 526
[101] Boisvert G and Lewis L J 1997 *Phys. Rev.* B **56** 7643
[102] Kellogg G L 1997 *Phys. Rev. Lett.* **79** 4417
[103] Ehrlich G and Hudda F G 1966 *J. Chem. Phys.* **44** 1039
[104] Schwoebel R J and Shipsey E J 1966 *J. Appl. Phys.* **37** 3682
[105] Gölzhäuser A and Ehrlich G 1996 *Phys. Rev. Lett.* **77** 1334
[106] Giesen M 2001 *Prog. Surf. Sci.* **68** 1
[107] Camarero J, de la Figuera J, de Miguel J J, Miranda R, Álvarez J and Ferrer S 2000 *Surf. Sci.* **459** 191
[108] Köhler U, Jensen C, Wolf C, Schindler A C, Brendel L and Wolf D E 2000 *Surf. Sci.* **454–456** 676
[109] Camarero J, Ferrón J, Cros V, Gómez L, Vázquez de Parga A L, Gallego J M, Prieto J E, de Miguel J J and Miranda R 1998 *Phys. Rev. Lett.* **81** 850
[110] Ferrón J, Gómez L, Gallego J M, Camarero J, Prieto J E, Cros V, Vázquez de Parga A L, de Miguel J J and Miranda R 2000 *Surf. Sci.* **459** 135
[111] Camarero J, Spendeler L, Schmidt G, Heinz K, de Miguel J J and Miranda R 1994 *Phys. Rev. Lett.* **73** 2448
[112] Vázquez de Parga A L, Vidal F J and Miranda R 2000 *Phys. Rev. Lett.* **85** 4365
[113] Müller S, Kostka G, Schäfer T, de la Figuera J, Prieto J E, Ocal C, Miranda R, Heinz K and Müller K 1996 *Surf. Sci.* **352–354** 46
[114] Camarero J, Cros V, Capitán M J, Álvarez J, Ferrer S, Niño M A, Prieto J E, Gómez L, Ferrón J, Vázquez de Parga A L, Gallego J M, de Miguel J J and Miranda R 1999 *Appl. Phys.* A **69** 553
[115] Camarero J, Niño M A, Farías D, Cros V, de Miguel J J, Miranda R, Hernando-Mañeru A, Asenjo A, González J M and Vázquez M 2001 *Surf. Sci.* **482–485** 1077
[116] van Leeuwen C, van Rosmalen R and Bennema P 1974 *Surf. Sci.* **44** 213
[117] Rusponi S, Costantini G, Boragno C and Valbusa U 1998 *Phys. Rev. Lett.* **81** 4184
[118] Rusponi S, Costantini G, Buatier de Mongeot F, Boragno C and Valbusa U 1999 *Appl. Phys. Lett.* **75** 3318
[119] Boragno C, Buatier de Mongeot F, Costantini G, Valbusa U, Felici R, Smilgies D-M and Ferrer S 2002 *Phys. Rev.* B **65** 153406
[120] Ritter M, Stindtmann M, Farle M and Baberschke K 1996 *Surf. Sci.* **348** 243
[121] Rusponi S, Costantini G, Boragno C and Valbusa U 1998 *Phys. Rev. Lett.* **81** 2735 and references herein
[122] Das Sarma S 1998 *Morphological Organization in Epitaxial Growth and Removal (Series on Directions on Condensed Matter Physics vol 14)* (Singapore: World Scientific) p 94
[123] Bartelt M C and Evans J W 1994 *Surf. Sci.* **314** L829
[124] Bales G S and Zangwill A 1990 *Phys. Rev.* B **41** 5500
[125] Mullins W W and Sekerka R F 1963 *J. Appl. Phys.* **34** 323
Mullins W W and Sekerka R F 1963 *J. Appl. Phys.* **35** 444
[126] Nelson R C, Einstein T L, Khare S V and Rous P J 1993 *Surf. Sci.* **1993** 462
[127] Liu S and Metiu H 1996 *Surf. Sci.* **359** 245
[128] Jacobsen J, Jacobsen K W and Nørskov J K 1996 *Surf. Sci.* **359** 37
[129] Liu C L and Adams J B 1992 *Surf. Sci.* **265** 262
[130] Krug J 1997 *Adv. Phys.* **46** 139
[131] Barabási A-L and Stanley H E 1995 *Fractal Concepts in Surface Growth* (Cambridge: Cambridge University Press)
[132] Wolf D and Villain J 1990 *Europhys. Lett.* **13** 389
[133] Vicsek T 1989 *Fractal Growth Phenomena* (Singapore: World Scientific)
[134] Das Sarma S and Tamborenea P I 1991 *Phys. Rev. Lett.* **66** 325
Tamborenea P I, Lai Z W and Das Sarma S 1992 *Surf. Sci.* **267** 1
[135] Ferrón J, de Miguel J J, de la Figuera J, Prieto J E, Camarero J, Cros V and Miranda R 1996/97 *Bulgarian Chem. Commun.* **29** 558
[136] Foiles S M, Baskes M I and Daw M S 1986 *Phys. Rev.* B **33** 7983
[137] de Miguel J J 1997 *Surf. Rev. Lett.* **4** 353
[138] Romé de l'Isle J B 1783 *Cristallographie* vol 1 (Paris: Imprimerie de Monsieur) p 379
[139] Cabrera N and Vermilyea D A 1958 *The Growth of Crystals from Solutions* (New York: Wiley) p 393
[140] Steigerwald D A, Jacob I and Egelhoff W F Jr 1988 *Surf. Sci.* **202** 472
[141] Egelhoff W F Jr and Steigerwald D A 1989 *J. Vac. Sci. Technol.* A **7** 2167
[142] Copel M, Reuter M C, Kaxiras E and Tromp R M 1989 *Phys. Rev. Lett.* **63** 632

[143] Egelhoff W F Jr, Chen P J, Powell C J, Stiles M D and McMichael R D 1996 *J. Appl. Phys.* **79** 2491
[144] Egelhoff W F Jr, Chen P J, Powell C J, Stiles M D, McMichael R D, Lin C-L, Sivertsen J M, Judy J H, Takano K and Berkowitz A E 1996 *J. Appl. Phys.* **80** 5183
[145] Egelhoff W F Jr, Chen P J, Powell C J, Stiles M D, McMichael R D, Judy J H, Takano K and Berkowitz A E 1997 *J. Appl. Phys.* **82** 6142
[146] Yang D X, Shashishekar B, Chopra H D, Chen P J and Egelhoff W F Jr 2001 *J. Appl. Phys.* **89** 7121
[147] LeGoues F K, Horn-von Hoegen M, Copel M and Tromp R M 1991 *Phys. Rev.* B **44** 12 894
[148] van der Vegt H A, van Pinxteren H M, Lohmeier H, Vlieg E and Thornton J M C 1992 *Phys. Rev. Lett.* **68** 3335
[149] van der Vegt H A, Huisman W J, Howes P B and Vlieg E 1995 *Surf. Sci.* **330** 101
[150] van der Vegt H A, Breeman M, Ferrer S, Etgens V H, Torrelles X, Fajardo P and Vlieg E 1995 *Phys. Rev.* B **51** 14 806
[151] Tölkes C, Struck R, David R, Zeppenfeld P and Comsa G 1998 *Appl. Phys. Lett.* **73** 1059
[152] Wolter H, Schmidt M and Wandelt K 1993 *Surf. Sci.* **298** 173
[153] Barabási A-L 1993 *Phys. Rev. Lett.* **70** 4102
[154] Meyer J A, Vrijmoeth J, van der Vegt H A, Vlieg E and Behm R J 1995 *Phys. Rev.* B **51** 14 790
[155] Oppo S, Fiorentini V and Scheffler M 1993 *Phys. Rev. Lett.* **71** 2437
[156] Tersoff J, Denier van der Gon A W and Tromp R M 1994 *Phys. Rev. Lett.* **72** 266
[157] Zhang Z Y and Lagally M G 1994 *Phys. Rev. Lett.* **72** 693
[158] Markov I 1994 *Phys. Rev.* B **50** 11 271
[159] Meyer J A, van der Vegt H A, Vrijmoeth J, Vlieg E and Behm R J 1996 *Surf. Sci. Lett.* **355** L375
[160] Vrijmoeth J, van der Vegt H A, Meyer J A, Vlieg E and Behm R J 1994 *Phys. Rev. Lett.* **72** 3843
[161] Rosenfeld G, Servaty R, Teichert C, Poelsema B and Comsa G 1993 *Phys. Rev. Lett.* **71** 895
[162] Esch S, Hohage M, Michely T and Comsa G 1994 *Phys. Rev. Lett.* **72** 518
[163] Prieto J E, Rath Ch, Müller S, Hammer L, Heinz K and Miranda R 2000 *Phys. Rev.* B **62** 5144
[164] Villarba M and Jónsson H 1994 *Surf. Sci.* **317** 15
[165] Camarero J, Álvarez J, Ferrer S, de Miguel J J and Miranda R unpublished data
[166] van der Vegt H A, Álvarez J, Torrelles X, Ferrer S and Vlieg E 1995 *Phys. Rev.* B **52** 17 443
[167] Camarero J, Vázquez de Parga A L, Prieto J E, de Miguel J J, Miranda R, Slutzky C, Ferrón J and Gómez 2002 Atomistic aspects of epitaxial growth *Proc. NATO Advanced Research Workshop (NATO Series II vol 65)* ed M Kotrla *et al* (Dordrecht: Kluwer) p 477
[168] Schneider C M, Bressler P, Schuster P, Kirschner J, de Miguel J J and Miranda R 1990 *Phys. Rev. Lett.* **64** 1059
[169] Fruchart O, Klaua M, Barthel J and Kirschner J 1999 *Phys. Rev. Lett.* **83** 2769
[170] Baibich M N 1996 *Magnetism, Magnetic Materials and their Applications Proc. III Latin American Workshop* (Singapore: World Scientific) p 69
[171] Moruzzi V L, Marcus P M and Kübler J 1989 *Phys. Rev.* B **39** 6957
[172] Jenniches H, Shen J, Mohan Ch-V, Manoharan S S, Barthel J, Ohresser P, Klaua M and Kirschner J 1999 *Phys. Rev.* B **59** 1196
[173] Ohresser P, Shen J, Barthel J, Zheng M, Mohan Ch-V, Klaua M and Kirschner J 1999 *Phys. Rev.* B **59** 3696
[174] Newkirk J B 1957 *Trans. Am. In. Min., Metall. Pet. Engr.* **212** 1214
[175] Abrahams S C, Guttman L and Kasper J S 1962 *Phys. Rev.* **127** 2052
[176] Niño M A, Farías D, de Miguel J J and Miranda R 2002 to be published
[177] Parkin S S P, Bhadra R and Roche K P 1991 *Phys. Rev. Lett.* **66** 2152
[178] Kohlhepp J, Cordes S, Elmers H J and Gradmann U 1992 *J. Magn. Magn. Mater.* **111** L231
[179] Egelhoff W F Jr and Kief M T 1992 *Phys. Rev.* B **45** 7795
[180] Camarero J, Graf T, de Miguel J J, Miranda R, Kuch W, Zharnikov M, Dittschar A, Schneider C M and Kirschner J 1996 *Phys. Rev. Lett.* **76** 4428
[181] Wulfhekel W, Lipkin N N, Kliewer J, Rosenfeld G, Comsa G, Jorritsma L C and Poelsema B 1996 *Surf. Sci.* **348** 227
[182] Markov V A, Pchelyakov O P, Sokolov L V, Stenin S I and Stoyanov S 1991 *Surf. Sci.* **250** 229
[183] Wulfhekel W, Beckmann I, Rosenfeld G, Poelsema B and Comsa G 1998 *Surf. Sci.* **395** 168
[184] Hinch B J, Koziol C, Toennies J P and Zhang G 1989 *Europhys. Lett.* **10** 341
[185] Schieffer P, Krembel C, Hanf M C and Gewinner G 1998 *Surf. Sci.* **400** 95
[186] Speller S, Degroote S, Deoster J, Langgouche G, Ortega J E and Närmann A 1998 *Surf. Sci.* **405** L542
[187] Hwang R Q 1996 *Phys. Rev. Lett.* **76** 4757
[188] Tober E D, Farrow R F C, Marks R F, Witte G, Kalki K and Chambliss D D 1998 *Phys. Rev. Lett.* **81** 1897
[189] Gambardella P, Blanc M, Kuhnke K, Kern K, Picaud F, Ramseyer C, Girardet C, Barreteau C, Spanjaard D and Desjonquères M C 2001 *Phys. Rev.* B **64** 045404

[190] Shchukin V A and Bimberg D 1999 *Rev. Mod. Phys.* **71** 1125
[191] Teichert C 2002 *Phys. Rep.* **365** 335
[192] STM image courtesy of Calleja F, Hinarejos J J and Vázquez de Parga A L
[193] Bartelt M C and Evans J W 1996 *Phys. Rev.* B **54** R17 359
[194] Yu C, Li D, Pearson J and Bader S D 2001 *Appl. Phys. Lett.* **78** 1228
[195] Tober E D, Ynzunza R X, Westphal C and Fadley C S 1996 *Phys. Rev.* B **53** 5444
[196] Shi H and Lederman D 2000 *J. Appl Phys.* **87** 6095